Glycolytic interference blocks influenza A virus propagation by impairing viral polymerase-driven synthesis of genomic vRNA

Authors: J. Kleinehr[1], K. Daniel[1], F. Günl[1], J. Janowski[1], L. Brunotte[1], M. Liebmann[2], M. Behrens[3], A. Gerdemann[3], L. Klotz[2], M. Esselen[3], H.-U. Humpf[3], S. Ludwig[1*#], E. R. Hrincius[1*]

Affiliations:

[1] Institute of Virology Muenster (IVM), Westfaelische Wilhelms-University Muenster, Von-Esmarch-Strasse 56, 48149 Muenster, Germany

[2] Department of Neurology with Institute of Translational Neurology, University Hospital Muenster, Albert-Schweitzer-Campus 1, 48149 Muenster, Germany

[3] Institute of Food Chemistry, Westfaelische Wilhelms-University Muenster, Corrensstrasse 45, 48149 Muenster, Germany

* Shared seniorauthorship

[#] **Correspondence:** Univ.-Prof. Dr. rer. nat. Stephan Ludwig, Institute of Virology Muenster, Von-Esmarch-Straße 56, 48149 Muenster, Germany, tel.: +492518357791, fax: +492518357793, ludwigs@uni-muenster.de

Running title: Glycolytic inhibition and influenza A virus replication

Abstract

Influenza A virus (IAV), like any other virus, provokes considerable modifications of its host cell's metabolism. This includes a substantial increase in the uptake as well as the metabolization of glucose. Although it is known for quite some time that suppression of glucose metabolism restricts virus replication, the exact molecular impact on the viral life cycle remained enigmatic so far. Using 2-deoxy-D-glucose (2-DG) we examined how well inhibition of glycolysis is tolerated by host cells and which step of the IAV life cycle is affected. We observed that effects induced by 2-DG are reversible and that cells can cope with relatively high concentrations of the inhibitor by compensating the loss of glycolytic activity by upregulating other metabolic pathways. Moreover, mass spectrometry data provided information on various metabolic modifications induced by either the virus or agents interfering with glycolysis. In the presence of 2-DG viral titers were significantly reduced in a dose-dependent manner. The supplementation of direct or indirect glycolysis metabolites led to a partial or almost complete reversion of the inhibitory effect of 2-DG on viral growth and demonstrated that indeed the inhibition of glycolysis and not of *N*-linked glycosylation was responsible for the observed phenotype. Importantly, we could show via conventional and strand-specific qPCR that the treatment with 2-DG led to a prolonged phase of viral mRNA synthesis while the accumulation of genomic vRNA was strongly reduced. At the same time, minigenome assays showed no signs of a general reduction of replicative capacity of the viral polymerase. Therefore, our data suggest that the significant reduction in IAV replication by glycolytic interference occurs mainly due to an impairment of the dynamic regulation of the viral polymerase which conveys the transition of the enzyme's function from transcription to replication.

Author Summary

Upon infection the influenza A virus alters the metabolism of infected cells. Among others, this includes a pronounced increase in glucose metabolism. We aimed to get a better understanding of these metabolic virus-host interactions and to unravel the mechanism by which glycolytic inhibition impairs the viral life cycle. On the one hand, we observed a virus-induced upregulation of many glycolysis metabolites which could often be reversed by the administration of a glycolysis inhibitor. On the other hand, our data suggested that the inhibitor treatment severely impaired viral propagation by interfering with the regulation of the viral polymerase. This manifested in an extended phase of transcription, while replication was strongly reduced. Additionally, we assessed the safety and tolerability of the used drug in immortalized and primary cells. Our study sheds more light on metabolic virus-host interactions and provides a better understanding of metabolic interference as a potential host-targeted antiviral approach, which does not bear the risk of creating resistances.

1. Introduction

Influenza viruses (IVs) still constitute a major risk factor for the human health all over the globe. According to extrapolations, 3-5 million severe cases and up to half a million deaths occur on average during annual IV epidemics [1]. The influenza A virus (IAV) is of special interest since it has zoonotic and pandemic potential. The high mutation rate of the IV genome easily allows to develop resistances to antiviral treatments. Therefore, more and more research focuses on targeting cellular factors, which are indispensable for viral replication, to develop novel host-targeted antiviral strategies. Since viruses in general are intracellular parasites and thus have no metabolism on their own, they completely depend on the host cell's metabolism for their replication. Moreover, each type of virus reshapes the host cell's metabolism towards its specific needs by regulating – often increasing – the uptake of metabolites and the activity of certain metabolic pathways [2-6]. Frequently, this includes elevated activity of glycolysis, the pentose phosphate pathway (PPP), lipid metabolism and the generation of amino acids [3]. This was also demonstrated for IV infections. Altered activity or elevated levels of pathway intermediates of, among others, glutaminolysis [7-9], fatty acid synthesis (FAS) [7, 9], the PPP [7, 8], the hexosamine biosynthetic pathway [9] and the tricarboxylic acid (TCA) cycle [7, 8] were observed. However, especially an increased glycolytic rate and uptake of glucose has been described in various immortalized and primary cells after infection with IV as well as in the lungs of infected patients [7, 8, 10]. Direct inhibition of glycolysis or mediators of glycolysis led to a significant impairment of IV reproduction and spread [7, 11, 12]. Furthermore, the concentration of extracellular lactate increases during IV infections [8], suggesting the exploitation of aerobic glycolysis. This is indicative of the Warburg effect [13, 14], in which cells metabolize glucose rather to lactate instead of pyruvate despite the adequate availability of oxygen. In this scenario, which is also observed in tumors, cells depend more on glycolysis than oxidative phosphorylation for sufficient synthesis of adenosine triphosphate (ATP). On the one hand IV benefits from this by rapidly generating large amounts of biological building blocks for its replication and on the other hand an increased production of lactate inhibits the induction of type I interferons [15].

In our research we targeted the glucose metabolism with a special focus on the inhibition of glycolysis with the inhibitor 2-deoxy-D-glucose (2-DG), which has already been demonstrated to interfere with the formation of new infectious IV particles [11, 12, 16, 17]. Beside the competitive inhibition of glucose uptake, 2-DG inhibits the first two glycolytic enzymes hexokinase (HK) and glucose-6-phosphate isomerase (GPI), the latter being its primary target. Just like glucose, 2-DG will be phosphorylated at the C6 position by HK to 2-deoxy-D-glucose-6-phosphate (2-DG-6-P). 2-DG-6-P competitively inhibits GPI and cannot be further metabolized by this enzyme. The increasing concentration of 2-DG-6-P leads to a feedback that additionally inhibits hexokinase in an allosteric manner [18-22]. Moreover, 2-DG gets fraudulently incorporated into oligosaccharide chains needed for *N*-linked glycosylation of glycoproteins [23], partially preventing this post-translational modification [24] and hence affecting the proteins' folding and their functions. This inhibition is mainly conveyed by guanosine diphosphate (GDP)-2-DG into which 2-DG can be converted [25]. Thereby, 2-DG evidentially inhibits glycolysis and interferes with *N*-linked glycosylation. Here, we demonstrate the inhibitor's significant impact on the replication of IAV without causing irreversible damage to the host cells. Furthermore, we unraveled a major mechanism by which this treatment interferes with the viral life cycle and discuss the potential of metabolic interference to fight severe IAV infections.

2. Results

2-DG is well tolerated in cells and exhibits strong virus-restricting activity

Our first aim was to prove the virus-restricting potential of 2-DG in cell culture. First, we showed in plaque assays that the number of newly produced infectious IAV particles decreased significantly in a dose-dependent manner when 2-DG was applied directly after the infection of A549 cells (**Fig 1A**). This decrease became as strong as more than four orders of magnitude when the glucose/2-DG ratio was 1:1. Second, we observed a very similar 2-DG-mediated decrease for IAV nucleoprotein (NP)-positive cells via flow cytometry (**Fig S1A**). These data demonstrated the strong impairment of IAV reproduction and spread in the presence of 2-DG.

Next, we assessed the reversibility as well as metabolic and potential cytotoxic effects of the 2-DG treatment on cells. Here, it could be demonstrated that the strong antiviral effect of a 24 h treatment was quickly abolished once the inhibitor was removed (**Fig 1B**). The massive increase of viral titers after the replacement of 2-DG with inhibitor-free medium suggested the full reversibility of 2-DG-induced effects and indicated that there was no permanent cell damage which is also substantiated by the literature [11]. By performing lactate dehydrogenase (LDH) assays we detected no cytotoxicity within the range of used 2-DG concentrations (**Fig 1C**), as previously demonstrated in various cell lines including A549 [26, 27]. Moreover, we could even observe a beneficial effect of the 2-DG treatment for the survival of infected cells. With increasing 2-DG concentrations the total percentage of dead cells decreased significantly 24 hours post infection (hpi) (**Fig S1B**). However, the results of the LDH assays in combination with data obtained from trypan blue exclusions suggested a certain cytostatic effect, since even though the viability of all samples was not affected, total cell counts decreased with rising 2-DG concentrations (**Fig S1C+D**). In line with these results, a cytostatic effect of 2-DG has also been observed previously in other cells [27-29]. Furthermore, we investigated the effect of 2-DG on the metabolism in real-time via a Seahorse Analyzer. We observed a very rapid and significant reduction of the glycolytic proton efflux rate (glycoPER), which constitutes a direct read-out of the glycolytic rate (**Fig 1D**). Since a major factor to calculate the glycoPER is the extracellular acidification rate (ECAR), this decreased in a similar pattern as the glycoPER (**Fig 1E**). Simultaneously, the oxygen consumption rate (OCR) of 2-DG-treated cells increased quickly after the beginning of the treatment (**Fig 1F**). These data proved the partial inhibition of glycolysis by 2-DG in a dose-dependent manner and indicated that cells were able to cope with the treatment by compensating the loss of glycolytic activity by upregulating cellular respiration to generate energy.

In addition to evaluating the cytotoxicity of 2-DG, we also tested potential effects of 2-DG on the innate immune response and the cellular responsiveness to viral infections. For that purpose, we measured expression levels of the proinflammatory genes *interleukin-6* (*IL-6*) and *C-X-C motif chemokine ligand 8* (*CXCL8*, protein: IL-8) as well as the interferon-stimulated

genes (ISGs) *DExD/H-box helicase 58* (*DDX58*, protein: retinoic acid inducible gene I) and *myxovirus resistance gene A* (*MxA*) after stimulation with either cellular or viral RNA in the presence or absence of 2-DG (**Fig S1E-H**). We observed a mild to more pronounced induction of *IL-6* (**Fig S1E**) and *CXCL8* (**Fig S1F**) with increasing concentrations of 2-DG. This finding was consistent with a previous publication, reporting that nutrient shortage (also induced by 2-DG) triggers a cell response which resembles wound healing processes in cancer cells as well as in primary cells [26]. Moreover, the mild induction of proinflammatory cytokines in the presence of 2-DG might be attributed to the fact that the inhibitor can also impair glycosylation. This in turn gives rise to endoplasmic reticulum (ER) stress, elicited by deficient glycoproteins, consequently leading to the unfolded protein response (UPR) [23] which has been demonstrated to drive the production of proinflammatory cytokines [30]. On the other hand, we measured no clear differences in the expression of *DDX58* (**Fig S1G**) and *MxA* (**Fig S1H**) in the presence of lower 2-DG concentrations but a moderate and significant reduction of both ISGs at 25 mM of the inhibitor, when stimulated with viral RNA. Nevertheless, our data confirmed that the cells were well responsive to viral stimuli, regardless of the concentration of 2-DG that was applied.

Apart from the permanent cell line A549, key experiments were repeated in primary human bronchial epithelial cells (HBEpCs) and genuine human lung explants (**Fig S2A-E**). Since the used media for primary tissue contained less glucose, lower concentrations of the inhibitor were used. However, we still applied the same 2-DG/glucose ratio to human lung explants as in A549 experiments which led to a significant and dose-dependent reduction of viral titers (**Fig S2A**). Because HBEpCs were more susceptible to the treatment, lower 2-DG/glucose ratios were applied. The highest concentration used in HBEpC experiments was 1200 µM which corresponds to the 2-DG/glucose ratio (1:5) of 5 mM 2-DG in experiments carried out with A549 cells. Similar to A549 cells, HBEpCs displayed barely any signs of cytotoxicity after treatment (**Fig S2B**). Reduced lactate concentrations in the supernatant of treated cells indirectly indicated the efficiency of glycolytic inhibition (**Fig S2C**). Importantly, the treatment with 2-DG also led to a significant and dose-dependent reduction of viral titers in HBEpCs (**Fig**

S2D+E). Even though the magnitude of the inhibitory effect on glycolysis and viral replication differed slightly from the data obtained with A549 cells – most likely due to distinct cellular metabolic activities and lower 2-DG/glucose ratios (HBEpC) – these data suggested the save use and antiviral activity of 2-DG in primary tissue.

2-DG only moderately affects viral protein translation in a single viral life cycle

Given the remarkable impairment of IAV replication by 2-DG, we now aimed to identify the spot of interference of the drug within the viral life cycle. Therefore, we checked potential changes in the accumulation of various IAV proteins 24 hpi (**Fig 2A**) and after a single replication cycle of 8 h (**Fig 2B**). In accordance with the strongly reduced viral titers there was also a pronounced reduction of viral protein accumulation after 24 h. However, within a single replication cycle we only detected rather weak differences among the accumulation of viral proteins. While the accumulation of the late viral proteins polymerase acidic protein (PA) and matrix protein 1 (M1) was moderately reduced, the accumulation of the early proteins NP and non-structural protein 1 (NS1) was barely affected by 2-DG. Consequently, even though there was a moderate reduction of some viral proteins within a single replication cycle we did not consider reduced viral protein accumulation to be the main reason for the severe impact of 2-DG on IAV propagation.

To rule out a general effect on the cellular protein synthesis machinery, we measured the fluorescence signal of the reporter *Renilla* luciferase driven by a constitutive promoter in a luciferase assay in the absence or presence of various concentrations of 2-DG (**Fig 2C**). Decreased signals would be an indication for an impairment of cellular transcription and/or translation. Interestingly, there was no negative effect on the luciferase signal, suggesting no general impairment of the cellular protein synthesis. Quite the opposite was the case when high concentrations of 2-DG were used which even led to an increase of the luciferase signal.

Glycolytic interference prolongs the phase of viral transcription while it clearly reduces viral replication within a replication cycle

After disproving viral protein expression being notably hampered by 2-DG, we delved deeper into the IAV replication cycle to understand the virus-restricting properties of 2-DG. Therefore, we now examined if a treatment with 2-DG interfered with the main processes driven by the viral polymerase: transcription and replication. Since IAV is a negative-sense RNA virus its RNA-dependent RNA polymerase can, right after reaching the host cell's nucleus, transcribe positive-sense mRNA. After translation and nuclear import, nascent viral polymerase complexes mediate the two-step process of replication. Here, a positive-sense, full-length complementary RNA (cRNA) is synthesized from the initial viral genomic RNA (vRNA) which subsequently serves as a template for vRNA synthesis [31, 32].

We analyzed the accumulation of viral mRNA and vRNA that codes for M1. In case of vRNA detection, the values of M1 are representative of segment 7 (M). As before, M1 mRNA and vRNA were analyzed after 24 h (**Fig 3A+B**) and after a single replication cycle of 8 h (**Fig 3C+D**) with and without 2-DG. As observed for viral proteins, we measured a massive reduction of M1 mRNA and vRNA 24 hpi when 2-DG was applied (**Fig 3A+B**), which is in line with the reduction of viral titers. Experiments for the duration of a single replication cycle, however, revealed intriguing differences between the two distinct RNA species. While viral mRNA levels were elevated in the presence of 2-DG (**Fig 3C**) the amount of vRNA was clearly reduced after an infection period of 8 h (**Fig 3D**). Again, these experiments were repeated with HBEpCs to see if there are similar effects in non-transformed cells with no altered metabolism (**Fig S2F-I**). Using these primary cells, we observed a very similar pattern of IAV mRNA and vRNA accumulation through the treatment with 2-DG as in A549 cells. While mRNA was decreased 24 hpi (**Fig S2F**) and unaffected 8 hpi (**Fig S2G**), vRNA was decreased at both time points (**Fig S2H+I**). The difference in mRNA accumulation 8 hpi might be due to a milder 2-DG treatment or could be a cell-specific effect. Nevertheless, the strong reduction in vRNA accumulation, limiting viral propagation, seemed to be tissue-independent.

With this phenotype at hand, we wanted to exclude a virus strain-specific effect and additionally analyzed the influence of 2-DG on viral growth, transcription, and replication of the H3N2 strain A/Panama/2007/1999 (Pan/99). As for SC35M, we observed a strong dose-dependent

decrease of viral titers, mRNA and vRNA 24 hpi (**Fig S3A-C).** Importantly, with an increase of Pan/99 mRNA and a decrease of vRNA in a single cycle experiment **(Fig S3D+E)** the results resembled those obtained with SC35M. Therefore, glycolytic interference on IAV appears to be a general phenomenon and not a virus strain-specific effect.

Summing up the obtained insights, the qPCR data suggested that the main cause for the impairment of IAV reproduction and spread by 2-DG is the interference of the inhibitor with the production of viral genome copies. Hereafter, we were especially interested in why glycolytic inhibition increased viral mRNA but decreased vRNA within a single viral life cycle.

In order to shed light on this question we performed an 8 h infection kinetic and analyzed the synthesis of M1 mRNA and vRNA in the presence of 2-DG in comparison to an untreated control (**Fig 4A+B**). In untreated cells the production of viral mRNA reached its strongest incline at approximately 6 hpi and started to establish a plateau afterwards (**Fig 4A**, black line). In contrast, the treatment with 2-DG led to a continuous increase of mRNA transcription, exceeding the total accumulation of viral mRNA in untreated cells (**Fig 4A**, gray line). Thus, despite a lower accumulation rate of viral mRNA in treated cells in the first 6 h of an infection, these samples displayed higher mRNA levels at time points later than 7 hpi. Even though the underlying mechanisms are unknown this observation explained why we detected higher viral mRNA levels in 2-DG-treated cells after one replication cycle (**Fig 3C**). In accordance with our previous data on vRNA accumulation at 8 hpi (**Fig 3D**), the kinetic revealed that vRNA accumulated at a clearly reduced rate when 2-DG was applied throughout the whole experiment (**Fig 4B**, gray line). To verify our results, we performed strand-specific real-time qPCR according to the protocol established by Kawakami *et al.* [33] for segment 5 (NP) and 6 (NA). Additionally, we analyzed segment 1 (PB2), which is the longest of the IAV gene segments, to rule out effects which might be caused by the length of different segments. We determined the n-fold of viral mRNA and vRNA of the three segments in 2-DG-treated cells 8 hpi in comparison to untreated cells. The results for all three gene segments were very similar and supported the previous kinetics. We observed a 3-4-fold increase of viral mRNA (**Fig 4C-E**) while the vRNA of the same gene segments was decreased by approximately 80-90%

(**Fig 4F-H**) when 2-DG was applied. Notably, these findings confirmed our previous measurements of mRNA and vRNA after one replication cycle (**Fig 3C+D**). The data presented in **Fig 4** indicated that glycolytic inhibition by 2-DG prolonged the phase of viral mRNA transcription while it attenuated viral genome replication. This suggested either a distinct effect on the transcriptional and replicative capacity of the viral polymerase or an impairment of the dynamic regulation of the polymerase function, determining whether it performs transcription or replication.

2-DG treatment does not affect the replicative capacity of the viral polymerase nor the durability of vRNA

After revealing that reduced vRNA accumulation in the presence of 2-DG was the most crucial consequence of glycolytic interference for viral growth, we wanted to understand this phenomenon more mechanistically. Minigenome systems can be used to explicitly focus on transcription and replication without the dynamic of a full-fledged infection and hence allow to dissect distinct steps of the viral life cycle to a certain degree. Here, minigenome assays were performed as described previously [34] to assess whether 2-DG has a direct influence on the activity of the viral polymerase. For this purpose, we transfected HEK293T cells with plasmids encoding all proteins of the viral ribonucleoprotein (vRNP) complex – PA, PB1, PB2 and NP – together with a reporter plasmid coding for a firefly luciferase under the control of a viral promoter. Another plasmid that constitutively expressed *Renilla* luciferase was co-transfected to serve as a transfection control. Subsequently, those cells were mock-treated or treated with 2-DG and analyzed via luciferase assay. By transfecting two different expression plasmids of the firefly reporter luciferase either vRNA-like or cRNA-like RNA templates were synthesized, which were converted by the transfected and nascent viral proteins. Thus, we were able to analyze the effect of 2-DG on the transcriptional capacity of the viral polymerase (**Fig 5A**) or a potential effect on the replicational capacity of the polymerase since vRNA first had to be synthesized from the cRNA-like template (**Fig 5B**). We observed that transcription was significantly reduced in the presence of 2-DG (**Fig 5A**) which confirms the previously seen

2-DG-induced lower accumulation rate of viral mRNA in the earlier phase of the 8 h kinetic (**Fig 4A**). On the other hand, there was no significant difference of the luciferase signal between the various samples when the cRNA plasmid was transfected (**Fig 5B**). Even though the interpretation here is less straightforward, since the transcription of vRNA in mRNA was also included in this process, this suggested no reduction of the replicational capacity of the viral polymerase by 2-DG.

Additionally, we examined whether the 2-DG treatment potentially affected the durability (e.g., altered stability or rate of degradation) of RNP complexes and performed an assay based on a previous publication [35] in which HEK293T cells were pre-transfected with plasmids encoding all RNP complex proteins. 24 h later they were infected with IAV and subsequently treated with 2-DG and cycloheximide, an inhibitor of translation, for 6 h. This way, the pre-transfected RNP proteins were synthesized and, after IAV infection, formed RNP complexes with the nascent cRNA and vRNA. Strand-specific real-time qPCR revealed that levels of vRNA remained equal between the solvent control and 2-DG-treated samples (**Fig S4**), which indicated no effect of 2-DG on the durability of vRNP complexes.

The data presented in the last two chapters suggested that 2-DG mainly impaired IAV replication and spread by interfering with viral genome replication which was marked by massively reduced levels of vRNA if the inhibitor was applied. However, 2-DG neither had a direct effect on the replicative capacity of the viral polymerase (**Fig 5B**) nor on the durability of vRNP complexes (**Fig S4**).

IAV infections and glycolytic interference alter the metabolic profile of A549 cells

Given the fact that viral infections affect the cellular metabolism and after revealing that the IAV life cycle is mainly impaired on the level of vRNA synthesis by glycolytic interference, we wanted to get a more comprehensive understanding of metabolic alterations induced by the virus and by a treatment with 2-DG. As we know from the literature [7-9], an IAV infection has profound impacts on the host's metabolism which especially applies to the glucose metabolism. Since IAV upregulates the glucose metabolism and 2-DG inhibits glycolysis, we

307 expected a (partial) reversion of virus-induced metabolic changes through the inhibitor.
308 Moreover, we were interested in metabolic changes aside from glycolysis. Via hydrophilic
309 interaction liquid chromatography (HILIC) coupled to tandem mass spectrometry (MS/MS), as
310 described previously [36], we analyzed major alterations of the metabolic profile of A549 cells,
311 induced by IAV infection and/or the treatment with 2-DG after 24 h (**Fig 6**).
312 In accordance with the literature [7, 8, 10], the levels of glucose and most detected glycolysis
313 intermediates were increased in infected cells, pointing towards an increase of the uptake of
314 glucose and the rate of glycolytic activity. When 2-DG was applied, several glycolytic
315 intermediates (e.g., glucose-6-phosphate (G-6-P) or F-6-P) were detected at decreased
316 concentrations in both, infected and uninfected cells. Counterintuitively, the amount of lactate
317 was decreased in infected cells, which may be explained by an increased efflux upon infection
318 [7, 8] or its metabolization into other intermediates. Independent of an infection, the treatment
319 with 2-DG clearly decreased intracellular lactate. Altogether our data confirmed a
320 virus-mediated upregulation of glycolysis as well as its downregulation in the presence of
321 2-DG. In combination with our previous data this strengthens the position of metabolic
322 inhibitors as effective antivirals by counteracting virus-induced alterations of the host
323 metabolism.
324 Other metabolic pathways which are closely connected to glycolysis, such as the PPP or the
325 TCA cycle, revealed some fascinating changes induced by 2-DG treatment or an IAV infection.
326 Among all analyzed metabolites 6-phosphogluconate (6-PG) exhibited the strongest increase
327 upon infection (> 8-fold). The supplementation of 2-DG increased 6-PG concentrations in
328 uninfected and infected cells. This suggested a strong redirection of G-6-P towards the PPP
329 which was probably actively induced by the virus or by the inhibition of GPI by 2-DG. It seems
330 that the oxidative branch of the PPP and thus the direct oxidation of glucose is upregulated
331 upon IAV infection. Similar results have been obtained previously in chicken embryo cells [10].
332 However, the profiles of detectable downstream intermediates of the non-oxidative PPP
333 differed from each other and were therefore difficult to interpret.

Most of the detected TCA cycle intermediates decreased upon inhibition of glycolysis (abolishment of the anaplerotic function of glycolysis) and during infection. The concentration of acetyl coenzyme A (acetyl-CoA), the linking intermediate between glycolysis and the TCA cycle, was increased in uninfected cells in the presence of 2-DG. But the highest increase of acetyl-CoA was found in untreated but infected cells. Apparently, IAV infections promote the production of large quantities of the important coenzyme.

Among amino acids we observed, with only a few exceptions (arginine, lysine and *N*-acetylaspartate), that most of them were decreased during infection. But, while 2-DG led to a decrease of approximately half of the analyzed amino acids it also induced a moderate increase of the other amino acids, independent of an infection. Besides, we noticed that ketogenic or partly ketogenic amino acids were barely or not reduced by 2-DG. Ketogenic amino acids can be catabolized into keto bodies (mostly TCA cycle intermediates such as acetyl-CoA, succinyl-CoA, or fumarate). The amino acids with most severely reduced concentrations after 2-DG treatment all belonged to the group of glucogenic amino acids, which means they can be catabolized into glucose through gluconeogenesis. In favor of this, we also found slightly increased concentrations of pyridoxine (vitamin B6), which is a co-factor for transaminase reactions which convert amino acids into substrates for gluconeogenesis [37, 38]. The inhibition of glycolysis by 2-DG feigned the deprivation of glucose and hence mimicked starvation. Probably this triggered cells to catabolize more glucogenic amino acids.

Furthermore, we observed a disturbance of the glutathione equilibrium, one of the most important antioxidant factors for cellular redox homeostasis. In line with this finding, the disruption of glutathione and consequentially the redox homeostasis, as an important factor for IAV pathogenicity, was described before [39-41].

The effect of an IAV infection and especially of 2-DG on many nucleobase-related metabolites (e.g., nucleobases, nucleosides and coenzymes with related structures) was rather mild. Despite the virus-mediated increase in glycolysis, just like Ritter *et al.* reported [8], we observed no significant alteration of ATP levels 24 hpi. Even though to a mild extent, the treatment with 2-DG had the expected effect on intracellular ATP in uninfected cells: 2-DG led

to an ATP decrease via inhibition of glycolysis (which even consumes ATP upstream of the inhibition of GPI through the ATP-driven phosphorylation of 2-DG to 2-DG-6-P). The increase of adenosine monophosphate (AMP) in the presence of 2-DG is supported by previous publications reporting of the activation of AMP-activated protein kinase (AMPK) after glycolytic inhibition, which is triggered by a low ATP/AMP ratio [22]. One of the most striking increases upon infection was the 6-fold increase of xanthine which was abolished if 2-DG was administered to infected cells. Despite the decrease of oxidized glutathione (GSSG), the virus-induced increase of xanthine might be linked to the generation of reactive oxygen species (ROS, in this case superoxide) which is an important factor for IAV pathogenicity and proliferation [42]. The catabolism of adenosine generates, among others, xanthine which in turn is a substrate for xanthine oxidase to generate superoxide [43]. In this light, a high catabolic rate of adenosine to generate xanthine during IAV infections may explain the low and high concentration of adenosine and xanthine, respectively, in infected but untreated cells.

Among miscellaneous metabolites we found three candidates which were distinctly affected. The first one is carnitine which is important for the mitochondrial shuttle of fatty acids for β-oxidation and thus the lipid metabolism. Interestingly, in infected but untreated cells carnitine was heavily decreased, suggesting a potential alteration of the lipid metabolism, which was earlier demonstrated in IBV-infected mice [44]. By inhibiting β-oxidation, the virus increases the pool of lipids which can be utilized for the viral envelope, biosynthesis and transport purposes. The other two striking metabolites were creatine and phosphocreatine which were moderately reduced upon IAV infection but heavily reduced in the presence of 2-DG. A main task of these molecules is the conversion of ADP into ATP to sustain energy levels. The strong downregulation of creatine and phosphocreatine might have correlated with the conspicuously mild impact of IAV and 2-DG on ATP concentrations by depleting creatine/phosphocreatine pools in order to maintain sufficient ATP levels.

All described measurements so far aimed to better understand IAV and 2-DG-induced metabolic alterations. However, beside these effects, we also analyzed samples which were additionally supplied with mannose, a C2 epimer of glucose. Since mannose can be converted

into fructose-6-phosphate (F-6-P) it should be able to bypass the inhibition by 2-DG to refuel glycolysis. Hence, we expected mannose to reverse some 2-DG-induced effects. Importantly, we observed this reversion, sometimes even followed by an increase, for several glycolytic intermediates (e.g., G-1-P, G-6-P and F-6-P) which demonstrated the antagonistic effect of mannose against glycolytic inhibition by 2-DG. The reduction of ATP in uninfected cells was reversed by mannose, too. However, mannose did not always reverse up-/downregulations of metabolites triggered by 2-DG. For instance, mannose could not or barely reverse the 2-DG-induced decreases of TCA cycle intermediates or alterations among PPP metabolites. Altogether, it seemed that the most pronounced reversions of 2-DG-mediated alterations on the metabolism by mannose took place among intermediates of the glucose metabolism and certain amino acids. Nevertheless, the supplementation of mannose sometimes affected metabolites apart from reversing 2-DG-mediated alterations.

Taken together, these data showed how diversely metabolic pathways are modified during IAV infections and that even metabolites from the same pathway may be affected in different manners. Furthermore, the complex connectivity between pathways or single metabolites became obvious once again. In the context of IAV infections it additionally suggested the potential of glycolytic interference to counteract IAV-induced metabolic changes as well as a function for mannose to regulate 2-DG-mediated effects.

Mannose circumvents the virus-restricting effect of 2-DG by refueling glycolysis

As described before, glycolysis is closely linked to various other metabolic pathways and its level of activity, as seen in **Fig 6**, can have a strong impact on the abundance of other metabolites. As shown in **Fig 7A** a very close connection exists to the mannose metabolism since F-6-P from glycolysis and mannose-6-phosphate can be converted into each other by the enzyme mannose-6-phosphate isomerase (MPI). Therefore, glucose and mannose should be able to substitute each other for many of their purposes inside a cell, which would also explain some results of the metabolomic data (**Fig 6**). Indeed, the vast majority of mannose is usually shunted to glycolysis to be catabolized. The remaining mannose is mainly utilized for

418 *N*-linked glycosylation [45]. Due to the close connection of glycolysis and *N*-linked
419 glycosylation and since others reported that the antiviral effect of 2-DG originated from the
420 impairment of glycosylation [25, 46] rather than glycolytic inhibition, we aimed to dissect the
421 interplay of these two hexoses in the context of IAV infections and the virus-restricting effects
422 of 2-DG. Since previous publications have shown that 2-DG reduced IAV glycoprotein
423 synthesis [24, 47] and that in general the inhibition of glycosylation by 2-DG could be reversed
424 by low doses of mannose [16, 48], we supplied 2-DG-treated cells with mannose to see if this
425 would reverse the inhibition of viral growth in our cell culture model as well (**Fig S5A**). Indeed,
426 low concentrations of mannose restored viral titers almost completely. We observed this
427 abolishment of the inhibitory function of 2-DG until a 1:10 ratio between mannose (1 mM) and
428 2-DG (10 mM). To elucidate if the reversal of inhibition can be attributed to mannose being
429 catabolized via glycolysis or being utilized for *N*-linked glycosylation we used the MPI inhibitor
430 MLS0315771 (MLS) to disrupt the link between these two pathways [49]. First, we determined
431 a safe dosage of the inhibitor including potential effects on cell growth, glycolysis, and the
432 formation of infective viral particles. We observed no significant effect on cell proliferation and
433 cell viability but an increase of lactate in the medium in the presence of 50 µM MLS, indicating
434 the safe use of the indicated concentrations and a higher glycolytic rate when the inhibitor is
435 applied (**Fig S5B-D**). The latter can be explained by the fact that MLS prevents the redirection
436 of F-6-P to *N*-linked glycosylation. Therefore, more glucose will be catabolized into lactate via
437 glycolysis. Besides, we observed no significant effect on the production of viral particles (**Fig**
438 **S5E**). Subsequently, we applied MLS to infected cells which were also treated with 2-DG and
439 mannose (**Fig 7B**). We saw the typical reduction of viral titers when 2-DG alone was applied
440 and the restoration of titers via the addition of mannose. Increasing concentrations of MLS
441 decreased viral titers back to the level of 2-DG-treated samples which suggested that mannose
442 restored IAV propagation mainly by driving glycolysis and not *N*-linked glycosylation.
443 Furthermore, it also confirmed that the inhibition of glycolysis was indeed the primary antiviral
444 mode of action of 2-DG. This got substantiated by the fact that the addition of pyruvate, the
445 final product of glycolysis under physiological conditions, partially restored viral titers after

inhibition by 2-DG (**Fig S5F**). To finally confirm the concept of the glycolytic rate as a determinant of IAV replication, we examined the effects of 2-DG, mannose, and MLS on the RNA levels of IAV after a single replication cycle of 8 h. The pattern of M1 vRNA accumulation (**Fig 7C**) strikingly resembled the pattern of viral titers (**Fig 7B**). The treatment with 2-DG led to a highly significant reduction of vRNA which was almost completely restored to the control value by supplementation of mannose. The additional administration of MLS, however, decreased the vRNA value to a similar extent as 2-DG alone did. Regarding viral mRNA accumulation (**Fig 7D**) we observed the typical slight increase after treatment with 2-DG, but barely a return to the control value when mannose was added as well. This only happened when also MLS was supplemented.

Summarizing, these data corroborated that the antiviral activity of 2-DG mainly derived from a strong impairment of the synthesis of viral genomic RNA by reducing the glycolytic rate of infected host cells. Moreover, by directly or indirectly inhibiting or fueling glycolysis we found a way to turn viral reproduction on and off to a certain degree.

3. Discussion

Understanding the diverse interplay between the host cell metabolism and viral intruders is of importance since it may create potential new strategies to counteract viral infections. In our study we were able to improve our comprehension of metabolic virus-host interactions as well as the mode of action of glycolytic interference on the life cycle of IAV. We observed profound changes of the whole metabolic profile of infected cells (**Fig 6**), including especially upregulated amounts of many intermediates of glycolysis. By applying 2-DG, a potent inhibitor of glycolysis, many virus-induced metabolic alterations could be reversed which indicated the inhibitor's counteraction against viral manipulations of the host. Furthermore, we showed the severe impact of glycolytic interference by 2-DG on the propagation of IAV *in vitro* (**Fig 1A+S1A**). The reduction of virus titers reached up to 4.5 orders of magnitude and hence was similar or even exceeded the effectivity of other antiviral compounds [50, 51].

During our search for the point of interference within the viral life cycle we deduced that viral protein synthesis played a subordinate role, because protein accumulation was rather mildly

affected within one replication cycle (**Fig 2B**). Interestingly, we did not at all observe a decrease in cellular protein accumulation after a 2-DG treatment, shown by steady signals of the cellular control protein in our western blots and via *Renilla* luciferase reporter assay (**Fig 2**). This may be indicative of a more selective effect which rather applies to viral than cellular protein translation. According to the data of **Fig 4** and **5** we assume that the predominant mechanism which is responsible for the strong reduction of IAV multiplication is a 2-DG-mediated interference with the dynamic regulation that switches the viral polymerase from a transcriptase to a replicase. Even though one hypothesis proposed that viral transcription and replication are stochastic without a switch mechanism [35] many studies suggest the opposite. The switch process of the polymerase is still not fully understood and is probably a multifactorial process determined by several viral and host factors (summarized in [31]). NP seems to be one of the key factors in this context and was shown to have a stimulatory function on viral polymerase activity via a direct interaction with it [52-55]. Additionally, NS1 and nuclear export protein (NEP, also known as NS2) are presumably implicated in viral replication [56-58]. Furthermore, small viral RNAs (svRNAs), which resemble the 5' end of vRNAs, have been linked to the regulation of viral replication [59-62]. It's been hypothesized that the role of svRNAs in viral replication is the association with a second and trans-acting polymerase which binds the 5' end of newly synthesized vRNA [31]. Even though it once was postulated that host factors are not required to initiate viral replication [54], many candidates that can associate with vRNP components [31, 55, 63-66] and thereby potentially influence the process, such as the recently described acidic nuclear phosphoprotein 32 (ANP32) [67-69], have been identified. Since the nuclear matrix and chromatin of infected cells were postulated to constitute a platform for viral transcription and replication [70-72], various potential host factors are associated with these sub-nuclear structures [73-76]. Linking the described regulators of IAV polymerase activity and the here presented data, it is quite possible that metabolic interference via 2-DG impairs the IAV replication-associated function or the expression of one or several of these viral or host factors. After all we know, however, it is also possible that there is no strong switching mechanism controlling viral transcription or replication. Potentially the abundance of

503 both processes is basically stochastic but can be modulated in favor of transcription or
504 replication in a time-dependent manner. Combining the insights from previous publications
505 with our data it is imaginable that the antiviral effect of 2-DG operates in several steps. One
506 scenario could be that inhibition by 2-DG leads to a primary antiviral effect by interfering with
507 the function of the initial transcription and replication complexes which could explain the
508 generalized lower levels of mRNA and vRNA until 7 hpi (**Fig 4**). A secondary effect could be
509 the seemingly selective impairment of the synthesis of some viral proteins. This includes at
510 least PA of the polymerase or RNP complex (**Fig 2B**). Consequently, a lack of nascent
511 polymerase complexes may have a stronger impact on replication than transcription since
512 replication requires a second polymerase for the binding of nascent cRNA and vRNA strands.
513 Alternatively or additionally, treatment with 2-DG might impair the synthesis of any of the
514 afore-mentioned modulators of the viral polymerase which may contribute to the prolonged
515 phase of transcription and the clear reduction of replication. Of course, the variety of potential
516 2-DG-mediated influences on viral replication is huge and on top of that we cannot fully exclude
517 an off-target interaction which may play a role here. However, the latter seems highly unlikely
518 based on the data we generated through the supplementation of mannose and MLS in the
519 presence of 2-DG (**Fig 7**). It will be interesting to examine if and how severely 2-DG influences
520 the expression or interactions of the afore-mentioned viral and cellular factors with the complex
521 replication machinery of IAV.
522 Furthermore, our data suggest that the predominant antiviral mode of action of 2-DG is the
523 inhibition of glycolysis. Decades ago it has been postulated that the impairment of *N*-linked
524 glycosylation is responsible for the antiviral effect of 2-DG [46]. The fact that inhibition of the
525 enzyme MPI, which links glycolysis and glycosylation, abolished the restoration of viral titers
526 and vRNA levels by mannose after treatment with 2-DG (**Fig 7B+C**) lets us oppose this view.
527 Our data indicate that the positive effect of mannose on IAV replication mainly (but not
528 necessarily exclusively) derives from fueling glycolysis via its conversion into F-6-P by MPI.
529 The partial recovery of the ATP/AMP ratio back to the physiological level in the presence of
530 2-DG and mannose (**Fig 6**) supports this theory. Moreover, the partial restoration of viral titers

by the supplementation of pyruvate after inhibiting glycolysis substantiates the assumption that glycolysis and its intermediates are crucial for virus reproduction. Probably the availability of glycolytic intermediates, which are needed to fuel other pathways and to synthesize macromolecules such as nucleotides and amino acids, is the most critical factor. Extrapolations predicted only a very minor extra demand for energy (~1% of the total energetic budget of a eukaryotic cell) to synthesize viral progeny during the characteristic time of an influenza infection [77]. Therefore, we assume that a potential role of ATP in viral replication may rather not be its availability for synthesis reactions.

As reviewed previously [78], 2-DG has various direct and indirect mechanism by which it can negatively affect normal cellular functions (e.g., inhibition of glycolysis and glycosylation or induction of AMPK and UPR). Therefore, a certain cytotoxicity – which heavily depends on the dose and type of administration as well as the type of cell, tissue, or organism – must be considered. However, we could demonstrate the tolerability and the quickness of effectivity of the antimetabolite in immortalized and primary cells (**Fig 1C-F, S1B, S2B+C**). Our *in vitro* data and previous reports [26, 27] support the performance of more *in vivo* studies and clinical trials to assess the safety of 2-DG and its efficiency to treat virus infections in model organisms or even humans. Several such studies have already reported the safety of 2-DG in animal models in the context of other virus infections [79] or different fields of research [80-82], especially when administered in continuous low doses. This could even be confirmed in clinical trials [83, 84]. Very recent phase II and III clinical trials in India [85, 86] demonstrated the safety and effectiveness of 2-DG when applied in addition to the standard of care to treat severe COVID-19 patients. As studies in which a virus infection was more successfully treated in humans through metabolic interference, these clinical trials may become a milestone in the development of host-targeted metabolic drugs as antivirals. However, some studies [87, 88] and its poor pharmacokinetic properties, e.g., its short plasma half-life [89], suggest that 2-DG itself may never become a licensed drug. Nevertheless, it is a useful tool to examine the principles of glycolytic interference and novel 2-DG analogs or other glycolytic inhibitors possibly boast a better pharmacological suitability [90]. Since dependence on the host

559 metabolism is a universal feature of all viruses, differential and strictly determined metabolic
560 treatments may be able to alleviate all types of virus infections in the future. However, before
561 this may become reality, we need to gain a more comprehensive understanding of
562 metabolism-related virus-host interactions, including virus-induced metabolic modifications,
563 specific metabolic needs of different viruses and how exactly metabolic treatments affect the
564 viral life cycle as well as the host. We are positive that this specific field of research deserves
565 more attention to elaborate metabolic interference and make it become a realistic and sensible
566 treatment option in the future.
567
568 **4. Experimental procedures**
569 **4.1 Cell lines and viruses**
570 Human adenocarcinomic alveolar basal epithelial cells (A549, American type culture collection
571 (ATCC®), CCL-185™) and human embryonic kidney (HEK) 293t cells (ATCC®, CRL-3216™)
572 were cultured in the high glucose variant of Dulbecco's modified Eagle's medium (DMEM,
573 Sigma-Aldrich, D5796) supplemented with 10 % fetal bovine serum (FBS). Madin-Darby
574 canine kidney (MDCK) II cells (Institute of Virology, WWU Muenster, Germany) were cultured
575 in minimum essential medium (MEM, Sigma-Aldrich, M4655) supplemented with 10 % fetal
576 bovine serum (FBS). The primary cells human bronchial epithelial cell (HBEpC, PromoCell,
577 C-12640) were cultured in airway epithelial cell growth medium (AECGM, PromoCell,
578 C-21060). Tumor-free human lung explants were obtained from various donors right after
579 surgery at the University Hospital Muenster and were cultured in Roswell Park Memorial
580 Institute-1640 medium (RPMI-1640, Sigma-Aldrich, R8758) supplemented with 100 U/mL
581 penicillin and 0.1 mg/mL streptomycin. The donors gave written consent for the tissue to be
582 used for scientific purposes. Ethical approval was given by the Deutsche Ärztekammer (AZ:
583 2016-265-f-S). All cells were kept at 37 °C and 5 % CO_2. Mouse-adapted
584 A/Seal/Massachusetts/1/80 H7N7 (SC35M) and A/Panama/2007/1999 H3N2 (Pan/99) are
585 recombinant influenza A virus (IAV) strains which were propagated in MDCK II cells.
586 **4.2 Infection and treatment**

Viruses were diluted to the desired multiplicity of infection (MOI) in phosphate-buffered saline (PBS) supplemented with 0.2 % bovine serum albumin (BSA), 1 mM $MgCl_2$, 0.9 mM $CaCl_2$, 100 U/mL penicillin and 0.1 mg/mL streptomycin. Cells were washed once with PBS and incubated for 30 min at 37 °C and 5 % CO_2 with the respective amount of virus. Afterwards A549 and HEK293T cells were washed once more with PBS and then incubated for the depicted periods in DMEM (Thermo Fisher Scientific, A14430) containing 0.2 % bovine serum albumin (BSA), 100 U/mL penicillin and 0.1 mg/mL streptomycin, 25 mM D-glucose, 2 mM L-glutamine and the respective concentration of inhibitor/supplement. The medium did not contain sodium pyruvate, HEPES and phenol red. HBEpCs were washed once with PBS after an infection and incubated in AECGM, containing the respective amounts of inhibitor/supplement for the depicted periods of the experiments. Human lung explants (~100 mg) were infected with 2 x 10^5 infectious virus particles as described previously [91], but without any interferon or bafilomycin. After washing the tissue 1 hpi, it was incubated in fresh RPMI supplemented with 2 mM L-glutamine, 100 U/mL penicillin, 0.1 mg/mL streptomycin, 0.1 % bovine serum albumin and the indicated concentrations of inhibitor. 2-deoxy-D-glucose (2-DG, Sigma-Aldrich, D8375), D-(+)-mannose (Sigma-Aldrich, M6020) and sodium pyruvate (Sigma-Aldrich, P5280) were dissolved in H_2O to 1 M (2-DG and mannose) and 2 M (sodium pyruvate) stock solutions. MLS0315771 (MedChemExpress, HY-112945) was dissolved in dimethyl sulfoxide (DMSO) to a stock concentration of 10 mM. For the stimulation of immune responses via RNA transfection, RNA was isolated from mock-infected and SC35M-infected (MOI of 5) cells 8 hpi, as described in **4.7**. 100 ng RNA per well was transfected using HiPerFect Transfection Reagent (QIAGEN) according to the manufacturer's protocol for 6 h in the presence of the depicted inhibitor concentrations.

4.3 Plaque titration

After the indicated periods of infection, the supernatants were collected and used to determine the number of infectious virus particles. Confluent MDCK II cells were infected with serial dilutions of the supernatants in PBS containing 0.2 % bovine serum albumin (BSA), 1 mM $MgCl_2$, 0.9 mM $CaCl_2$, 100 U/mL penicillin and 0.1 mg/mL streptomycin for 30 min at 37 °C

and 5 % CO_2. Subsequently the supernatants were replaced with MEM/BA containing 0.21 % BSA, 0.21 % $NaHCO_3$, 1 mM $MgCl_2$, 0.01 % DEAE-dextran, 0.9 mM $CaCl_2$, 100 U/ml penicillin, 0.1 mg/ml streptomycin and 0.9 % purified agar. After an incubation for 2-3 days at 37 °C and 5 % CO_2 the overlay was removed and cells were stained with a Coomassie staining solution (45 % ddH_2O (v/v), 45 % methanol (v/v), 10 % acetic acid (v/v) and 0.25 % Coomassie Brilliant blue R-250 (w/v)). Cell free plaques in the monolayer were counted as plaque-forming units per milliliter (PFU/mL).

4.4 Cytotoxicity assays

Potential cytotoxic effects of inhibitors were assessed by three different methods: lactate dehydrogenase (LDH) assay, trypan blue staining and flow cytometry. LDH assays were performed with the CytoSelect LDH cytotoxicity assay kit (Bio Cat, CBA-241-CB) according to the manufacturer's manual. Trypan blue exclusion was done by mixing a 0.4 % trypan blue dye (Invitrogen) 1:1 with a sample's cell suspension and having the automated cell counting machine Countess™ II (Invitrogen) determine the number of living cells. Determination of living cells via flow cytometry is described below in section **4.10**.

4.5 Glycolytic rate test

The induced assay version of the glycolytic rate test (Agilent, Kit 103344-100) was performed with a Seahorse XFe96 Analyzer (Agilent) according to the manufacturer's instructions. The assay medium was supplemented with 25 mM D-glucose and 2 mM L-glutamine to match other experimental conditions. Concomitantly, the final injection of 2-DG was set to 125 mM. After three measured points to obtain the basal glycolytic level, the indicated concentrations of inhibitor were injected and the glycolytic rate was measured for 1 h before continuing with the standard procedure.

4.6 Lactate assay

To determine the concentration of lactate in the supernatants of samples and thus have an indirect assay to assess glycolytic activity, the L-Lactate Assay Kit II (PK-CA577-K607) from PromoCell was used according to the manufacturer's instruction.

4.7 Reverse transcription and quantitative real-time PCR

643 At the end of an infection and/or treatment period, total RNA was isolated using the RNeasy®
644 Plus Mini Kit (Qiagen). The procedure was done according to the manufacturer's manual.
645 Reverse transcription was performed with the RevertAid™ H Minus Reverse Transcriptase
646 (Thermo Fisher Scientific) and oligo(dT) primers (Eurofins Genomics) for detection of mRNA
647 or a fluA uni12 forward primer [92] (Sigma-Aldrich, 5'-AGCAAAAGCAGG-3') to detect vRNA
648 according to the manufacturer's protocol. The obtained cDNA was used for real-time qPCR
649 with a LightCycler® 480 II (Roche) and Brilliant III SYBR® Green (Agilent) according to the
650 manufacturer's instructions. The following primers were used during qPCR: influenza matrix
651 protein M1 forward (5'-AGA TGA GTC TTC TAA CCG AGG TCG-3') and reverse (5'-TGC AAA
652 AAC ATC TTC AAG TCT CTG-3'), IL-6 forward (5'-AGA GGC ACT GGC AGA AAA CAA C-3')
653 and reverse (5'-AGG CAA GTC TCC TCA TTG AAT CC-3'), CXCL8 forward (5'-ACT GAG
654 AGT GAT TGA GAG TGG AC-3') and reverse (5'-AAC CCT CTG CAC CCA GTT TTC-3'),
655 DDX58 forward (5'-CCT ACC TAC ATC CTG AGC TAC AT-3') and reverse (5'-TCT AGG GCA
656 TCC AAA AAG CCA-3'), MxA forward (5'-GTT TCC GAA GTG GAC ATC GCA-3') and reverse
657 (5'-GAA GGG CAA CTC CTG ACA GT-3') and human glyceraldehyde 3-phosphate
658 dehydrogenase (GAPDH) forward (5'-GCA AAT TCC ATG GCA CCG T-3') and reverse
659 (5'-GCC CCA CTT GAT TTT GGA GG-3'). GAPDH, as a housekeeping gene, was used for
660 the normalization of PCR results. The relative n-fold was calculated using the $2^{-\Delta\Delta CT}$ method
661 [93].

662 **4.8 Strand-specific quantitative real-time RT-PCR**

663 Total RNA was isolate as described in **4.7**. Reverse transcription was performed by using
664 Maxima™ Reverse Transcriptase (Thermo Fisher Scientific) according to the manufacturer's
665 instructions and specific primers (Eurofins Genomics) for the different types of RNA as
666 reported previously [33]. The following primers were designed according to the SC35M
667 sequences DQ266097, DQ226096 and DQ266095 (Influenza Research Database) and used
668 for cDNA synthesis and qPCR of the SC35M segments 1, 5 and 6:

669 **Table 1: Primer for strand-specific real-time qPCR subdivided into their use in cDNA synthesis via reverse transcription**
670 **and PCR.**

target	purpose	primer name	sequence (5' - 3')	position (nt)

segment 1 (PB2)	vRNA	RT	vRNAtag_SC35M_seg1_1540F	GGCCGTCATGGTGGCGAAT CGGGATCAACGAGGGAATGTACTAC	1540-1564
		PCR	vRNAtag	GGCCGTCATGGTGGCGAAT	
			SC35M_seg1_1704R	AGTTTCCCAGTTCCTGATGATCCA	1704-1681
	mRNA	RT	mRNAtag_SC35M_seg1_dTR	CCAGATCGTTCGAGTCGT TTTTTTTTTTTTTTTTAAACAATTCGA	2325-2310
		PCR	mRNAtag	CCAGATCGTTCGAGTCGT	
			SC35M_seg1_2176F	GCGAAGGGAGAGAAGGCTAATGTGC	2176-2200
segment 5 (NP)	vRNA	RT	vRNAtag_SC35M_seg5_675F	GGCCGTCATGGTGGCGAAT AAATGGGCGGAGAACAAGAATTGC	675-698
		PCR	vRNAtag	GGCCGTCATGGTGGCGAAT	
			SC35M_seg5_845R	CTCAGAATGAGAGCAGACCGTGCA	845-822
	mRNA	RT	mRNAtag_SC35M_seg5_dTR	CCAGATCGTTCGAGTCGT TTTTTTTTTTTTTTTTCTTTAATTGTT	1549-1534
		PCR	mRNAtag	CCAGATCGTTCGAGTCGT	
			SC35M_seg5_1466F	CGATCGTGCCTTCCTTTGACATG	1466-1488
segment 6 (NA)	vRNA	RT	vRNAtag_SC35M_seg6_734F	GGCCGTCATGGTGGCGAAT GTAGTGATGACCGATGGATCAGCA	734-757
		PCR	vRNAtag	GGCCGTCATGGTGGCGAAT	
			SC35M_seg6_885R	CAAGTTACTTTTGAATCGTGCCCATAG	885-859
	mRNA	RT	mRNAtag_SC35M_seg6_dTR	CCAGATCGTTCGAGTCGT TTTTTTTTTTTTTTTTGCAATTTACGA	1445-1430
		PCR	mRNAtag	CCAGATCGTTCGAGTCGT	
			SC35M_seg6_1338F	GGTGGACGAGCAACAGCTTAGTTGC	1338-1362

4.9 Western blot

Samples were lysed at 4 °C with radioimmunoprecipitation assay (RIPA) buffer (25 mM Tris-HCl pH 8, 137 mM NaCl, 10 % glycerol, 0.1 % SDS, 0.5 % NaDOC, 1 % NP-40, 2 mM EDTA pH 8, 200 µM Pefabloc®, 5 µg/mL aprotinin, 5 µg/mL leupeptin, 1 mM sodium orthovanadate and 5 mM benzamidine). Cell debris was removed via centrifugation and protein concentrations were determined by Bradford assay. Samples were adjusted to the same protein concentration, mixed with the appropriate amount of Laemmli sample buffer and then proteins were separated and visualized by sodium dodecyl sulfate polyacrylamide gel electrophoresis (SDS-PAGE) and western blot analysis. The following primary antibodies were used to detect their respective proteins: ERK2 (rabbit, polyclonal, Santa Cruz, sc-154), M1 (mouse, monoclonal, Biorad, MCA401), NP (rabbit, polyclonal, GeneTex, GTX125989), NS1 (rabbit, polyclonal, GeneTex, GTX125990), and PA (rabbit, polyclonal, GeneTex, GTX125932). ERK2 served as the loading control for whole cell lysates. Fluorescence signals were visualized by using fluorophore-labelled secondary antibodies: IRDye® 680RD Donkey anti-Mouse (LI-COR, 926-68072), IRDye® 680RD Donkey anti-Rabbit (LI-COR, 926-68073), IRDye® 800CW Donkey anti-Mouse (LI-COR, 926-32212), and IRDye® 800CW Donkey

anti-Rabbit (LI-COR, 926-32213). Images were taken with the ODYSSEY® F_C Imaging System (LI-COR).

4.10 Flow Cytometry

At the end of an infection with or without treatment, cells were trypsinized and subsequently stained for analysis via flow cytometry with the FACSCalibur (Becton Dickinson) flow cytometer. At first, cells were stained with eBioscience™ Fixable Viability Dye eFluor™ 660 (Invitrogen, 65-0866-14) for 30 min at 4 °C in the dark. Afterwards the samples were fixated and permeabilized for 20 min and 60 min at 4 °C in the dark using BD Cytofix/Cytoperm™ solution and BD Perm/Wash™ solution (BD Biosciences), respectively. Intracellular staining of influenza A nucleoprotein was done by applying the anti influenza A (nucleoprotein) – FITC antibody (OriGene, AM00924FC-N) for 60 min at 4 °C in the dark. FlowJo software v10 (Becton Dickinson) was used to analyze the data obtained by flow cytometry. 10^5 cells of each sample were analyzed. The gating strategy is displayed in **Fig S6**.

4.11 Minigenome assay

Using Lipofectamine™ 2000 (Invitrogen), HEK293T cells were transfected with polymerase II-driven plasmids coding for PA, PB1, PB2, NP of SC35M as well as the transfection control *Renilla* luciferase. A sixth plasmid was one of two polymerase I-driven plasmids encoding either a vRNA-like or cRNA-like firefly luciferase template. 4 h post transfection the medium was replaced with DMEM (Thermo Fisher Scientific, A14430) containing 0.2 % BSA, 100 U/mL penicillin and 0.1 mg/mL streptomycin, 25 mM D-glucose, 2 mM L-glutamine and the respective concentration of 2-DG. 24 h post transfection the Dual-Luciferase® Reporter Assay System (Promega) was used according to the manufacturer's manual. For measurements of relative light units (RLU) the luminometer MicroLumat*Plus* LB 96V (Berthold Technologies) and the software WinGlow (Berthold Technologies) were used.

4.12 RNP durability assay

HEK293T cells were transfected with plasmids coding for PA, PB1, PB2 and NP of SC35M using Lipofectamine™ 2000 (Invitrogen). 24 h post transfection cells were infected with SC35M at an MOI of 5 (see **4.2**) and incubated with or without cycloheximide (100 µg/mL) and various

716 concentrations of 2-DG. 6 hpi cell lysates were taken and subjected to strand-specific
717 quantitative real-time RT-PCR (see **4.8**).

718 **4.13 Metabolic profiling by HILIC-MS/MS**

719 24 h after seeding 1.5 x 10^6 A549 cells in 6 cm dishes, they were mock-infected or infected
720 with SC35M at an MOI of 0.001. 24 hpi cells were washed twice with PBS and 400 µL
721 pre-cooled (4-8 °C) acetonitrile (ACN)/water (4+1, v/v) including 50 µM D-phenylglycine as
722 internal standard was added for metabolic quenching. Until further preparation the samples
723 were kept at 4-8 °C. Cells were then detached using a sterile cell scraper. The dish was
724 washed with additional 800 µL ACN/water (4+1, v/v) and pooled with the respective cell
725 sample. Further preparation of samples as well as chromatographic and mass spectrometric
726 analysis were performed as described previously [36].

727

728 **5. Acknowledgement**

729 J.K is a member of CiM-IMPRS, the joint graduate school of the Cells in Motion Interfaculty
730 Centre, University of Muenster, Germany and the International Max Planck Research
731 School-Molecular Biomedicine, Muenster, Germany. Besides, we acknowledge technical
732 support from L. Schürmann.

References

1. Girard MP, Cherian T, Pervikov Y, Kieny MP. A review of vaccine research and development: human acute respiratory infections. Vaccine. 2005;23(50):5708-24.
2. Sanchez EL, Lagunoff M. Viral activation of cellular metabolism. Virology. 2015;479-480:609-18.
3. Thaker SK, Ch'ng J, Christofk HR. Viral hijacking of cellular metabolism. BMC Biol. 2019;17(1):59.
4. Mayer KA, Stockl J, Zlabinger GJ, Gualdoni GA. Hijacking the Supplies: Metabolism as a Novel Facet of Virus-Host Interaction. Front Immunol. 2019;10:1533.
5. Moreno-Altamirano MMB, Kolstoe SE, Sanchez-Garcia FJ. Virus Control of Cell Metabolism for Replication and Evasion of Host Immune Responses. Front Cell Infect Microbiol. 2019;9:95.
6. Kleinehr J, Wilden JJ, Boergeling Y, Ludwig S, Hrincius ER. Metabolic Modifications by Common Respiratory Viruses and Their Potential as New Antiviral Targets. Viruses. 2021;13(10).
7. Smallwood HS, Duan S, Morfouace M, Rezinciuc S, Shulkin BL, Shelat A, et al. Targeting Metabolic Reprogramming by Influenza Infection for Therapeutic Intervention. Cell Rep. 2017;19(8):1640-53.
8. Ritter JB, Wahl AS, Freund S, Genzel Y, Reichl U. Metabolic effects of influenza virus infection in cultured animal cells: Intra- and extracellular metabolite profiling. BMC Syst Biol. 2010;4:61.
9. Tian X, Zhang K, Min J, Chen C, Cao Y, Ding C, et al. Metabolomic Analysis of Influenza A Virus A/WSN/1933 (H1N1) Infected A549 Cells during First Cycle of Viral Replication. Viruses. 2019;11(11).
10. Klemperer H. Glucose breakdown in chick embryo cells infected with influenza virus. Virology. 1961;13:68-77.
11. Kilbourne ED. Inhibition of influenza virus multiplication with a glucose antimetabolite (2-deoxy-D-glucose). Nature. 1959;183(4656):271-2.
12. Kohio HP, Adamson AL. Glycolytic control of vacuolar-type ATPase activity: a mechanism to regulate influenza viral infection. Virology. 2013;444(1-2):301-9.
13. Warburg O, Wind F, Negelein E. The Metabolism of Tumors in the Body. J Gen Physiol. 1927;8(6):519-30.
14. Warburg O. On the origin of cancer cells. Science. 1956;123(3191):309-14.
15. Thyrsted J, Storgaard J, Blay-Cadanet J, Heinz A, Thielke AL, Crotta S, et al. Influenza A induces lactate formation to inhibit type I IFN in primary human airway epithelium. iScience. 2021;24(11):103300.
16. Datema R, Schwarz RT. Interference with glycosylation of glycoproteins. Inhibition of formation of lipid-linked oligosaccharides in vivo. Biochem J. 1979;184(1):113-23.
17. Nakamura K, Compans RW. Effects of glucosamine, 2-deoxyglucose, and tunicamycin on glycosylation, sulfation, and assembly of influenza viral proteins. Virology. 1978;84(2):303-19.
18. Wick AN, Drury DR, Nakada HI, Wolfe JB. Localization of the primary metabolic block produced by 2-deoxyglucose. J Biol Chem. 1957;224(2):963-9.
19. Urakami K, Zangiacomi V, Yamaguchi K, Kusuhara M. Impact of 2-deoxy-D-glucose on the target metabolome profile of a human endometrial cancer cell line. Biomed Res. 2013;34(5):221-9.
20. Zhang D, Li J, Wang F, Hu J, Wang S, Sun Y. 2-Deoxy-D-glucose targeting of glucose metabolism in cancer cells as a potential therapy. Cancer Lett. 2014;355(2):176-83.

781 21. Pelicano H, Martin DS, Xu RH, Huang P. Glycolysis inhibition for anticancer treatment.
782 Oncogene. 2006;25(34):4633-46.
783 22. Pajak B, Siwiak E, Soltyka M, Priebe A, Zielinski R, Fokt I, et al. 2-Deoxy-d-Glucose and
784 Its Analogs: From Diagnostic to Therapeutic Agents. Int J Mol Sci. 2019;21(1).
785 23. Mesri EA, Lampidis TJ. 2-Deoxy-d-glucose exploits increased glucose metabolism in
786 cancer and viral-infected cells: Relevance to its use in India against SARS-CoV-2. IUBMB Life.
787 2021;73(10):1198-204.
788 24. Schwarz RT, Schmidt MF, Anwer U, Klenk HD. Carbohydrates of influenza virus. I.
789 Glycopeptides derived from viral glycoproteins after labeling with radioactive sugars. J Virol.
790 1977;23(2):217-26.
791 25. Schwarz RT, Schmidt MF, Datema R. Inhibition of glycosylation of viral glycoproteins.
792 Biochem Soc Trans. 1979;7(2):322-6.
793 26. Puschel F, Favaro F, Redondo-Pedraza J, Lucendo E, Iurlaro R, Marchetti S, et al.
794 Starvation and antimetabolic therapy promote cytokine release and recruitment of immune
795 cells. Proc Natl Acad Sci U S A. 2020;117(18):9932-41.
796 27. Bhatt AN, Kumar A, Rai Y, Kumari N, Vedagiri D, Harshan KH, et al. Glycolytic inhibitor
797 2-deoxy-d-glucose attenuates SARS-CoV-2 multiplication in host cells and weakens the
798 infective potential of progeny virions. Life Sci. 2022;295:120411.
799 28. Zhang XD, Deslandes E, Villedieu M, Poulain L, Duval M, Gauduchon P, et al. Effect of
800 2-deoxy-D-glucose on various malignant cell lines in vitro. Anticancer Res. 2006;26(5A):3561-
801 6.
802 29. Nef HM, Mollmann H, Joseph A, Troidl C, Voss S, Vogt A, et al. Effects of 2-deoxy-D-
803 glucose on proliferation of vascular smooth muscle cells and endothelial cells. J Int Med Res.
804 2008;36(5):986-91.
805 30. Smith JA. Regulation of Cytokine Production by the Unfolded Protein Response;
806 Implications for Infection and Autoimmunity. Front Immunol. 2018;9:422.
807 31. Te Velthuis AJ, Fodor E. Influenza virus RNA polymerase: insights into the mechanisms
808 of viral RNA synthesis. Nat Rev Microbiol. 2016;14(8):479-93.
809 32. Dou D, Revol R, Ostbye H, Wang H, Daniels R. Influenza A Virus Cell Entry, Replication,
810 Virion Assembly and Movement. Front Immunol. 2018;9:1581.
811 33. Kawakami E, Watanabe T, Fujii K, Goto H, Watanabe S, Noda T, et al. Strand-specific
812 real-time RT-PCR for distinguishing influenza vRNA, cRNA, and mRNA. J Virol Methods.
813 2011;173(1):1-6.
814 34. Te Velthuis AJW, Long JS, Barclay WS. Assays to Measure the Activity of Influenza Virus
815 Polymerase. Methods Mol Biol. 2018;1836:343-74.
816 35. Vreede FT, Jung TE, Brownlee GG. Model suggesting that replication of influenza virus
817 is regulated by stabilization of replicative intermediates. J Virol. 2004;78(17):9568-72.
818 36. Gerdemann A, Behrens M, Esselen M, Humpf HU. Metabolic profiling as a powerful
819 tool for the analysis of cellular alterations caused by 20 mycotoxins in HepG2 cells. Arch
820 Toxicol. 2022;96(11):2983-98.
821 37. Angel JF. Gluconeogenesis in meal-fed, vitamin B-6-deficient rats. J Nutr.
822 1980;110(2):262-9.
823 38. Nanbara S, Tanaka K, Koide H, Tanaka T, Hayashi T. Changes on levels of B6 vitamin
824 and aminotransferase in the liver of diabetic animals. Diabetes Res Clin Pract. 1990;9(2):109-
825 14.
826 39. Chen KK, Minakuchi M, Wuputra K, Ku CC, Pan JB, Kuo KK, et al. Redox control in the
827 pathophysiology of influenza virus infection. BMC Microbiol. 2020;20(1):214.

828 40. Lin X, Wang R, Zou W, Sun X, Liu X, Zhao L, et al. The Influenza Virus H5N1 Infection
829 Can Induce ROS Production for Viral Replication and Host Cell Death in A549 Cells Modulated
830 by Human Cu/Zn Superoxide Dismutase (SOD1) Overexpression. Viruses. 2016;8(1).
831 41. Suliman HB, Ryan LK, Bishop L, Folz RJ. Prevention of influenza-induced lung injury in
832 mice overexpressing extracellular superoxide dismutase. Am J Physiol Lung Cell Mol Physiol.
833 2001;280(1):L69-78.
834 42. Keshavarz M, Solaymani-Mohammadi F, Namdari H, Arjeini Y, Mousavi MJ, Rezaei F.
835 Metabolic host response and therapeutic approaches to influenza infection. Cell Mol Biol Lett.
836 2020;25:15.
837 43. Akaike T, Ando M, Oda T, Doi T, Ijiri S, Araki S, et al. Dependence on O2- generation by
838 xanthine oxidase of pathogenesis of influenza virus infection in mice. J Clin Invest.
839 1990;85(3):739-45.
840 44. Trauner DA, Horvath E, Davis LE. Inhibition of fatty acid beta oxidation by influenza B
841 virus and salicylic acid in mice: implications for Reye's syndrome. Neurology. 1988;38(2):239-
842 41.
843 45. Sharma V, Ichikawa M, Freeze HH. Mannose metabolism: more than meets the eye.
844 Biochem Biophys Res Commun. 2014;453(2):220-8.
845 46. Schwarz RT, Klenk HD. Inhibition of glycosylation of the influenza virus hemagglutinin.
846 J Virol. 1974;14(5):1023-34.
847 47. Klenk HD, Scholtissek C, Rott R. Inhibition of glycoprotein biosynthesis of influenza
848 virus by D-glucosamine and 2-deoxy-D-glucose. Virology. 1972;49(3):723-34.
849 48. Kurtoglu M, Gao N, Shang J, Maher JC, Lehrman MA, Wangpaichitr M, et al. Under
850 normoxia, 2-deoxy-D-glucose elicits cell death in select tumor types not by inhibition of
851 glycolysis but by interfering with N-linked glycosylation. Mol Cancer Ther. 2007;6(11):3049-
852 58.
853 49. Sharma V, Ichikawa M, He P, Scott DA, Bravo Y, Dahl R, et al. Phosphomannose
854 isomerase inhibitors improve N-glycosylation in selected phosphomannomutase-deficient
855 fibroblasts. J Biol Chem. 2011;286(45):39431-8.
856 50. Hamza H, Shehata MM, Mostafa A, Pleschka S, Planz O. Improved in vitro Efficacy of
857 Baloxavir Marboxil Against Influenza A Virus Infection by Combination Treatment With the
858 MEK Inhibitor ATR-002. Front Microbiol. 2021;12:611958.
859 51. Takahashi K, Furuta Y, Fukuda Y, Kuno M, Kamiyama T, Kozaki K, et al. In vitro and in
860 vivo activities of T-705 and oseltamivir against influenza virus. Antivir Chem Chemother.
861 2003;14(5):235-41.
862 52. Beaton AR, Krug RM. Transcription antitermination during influenza viral template RNA
863 synthesis requires the nucleocapsid protein and the absence of a 5' capped end. Proc Natl
864 Acad Sci U S A. 1986;83(17):6282-6.
865 53. Shapiro GI, Krug RM. Influenza virus RNA replication in vitro: synthesis of viral template
866 RNAs and virion RNAs in the absence of an added primer. J Virol. 1988;62(7):2285-90.
867 54. Newcomb LL, Kuo RL, Ye Q, Jiang Y, Tao YJ, Krug RM. Interaction of the influenza a virus
868 nucleocapsid protein with the viral RNA polymerase potentiates unprimed viral RNA
869 replication. J Virol. 2009;83(1):29-36.
870 55. Kawaguchi A, Momose F, Nagata K. Replication-coupled and host factor-mediated
871 encapsidation of the influenza virus genome by viral nucleoprotein. J Virol. 2011;85(13):6197-
872 204.
873 56. Marion RM, Zurcher T, de la Luna S, Ortin J. Influenza virus NS1 protein interacts with
874 viral transcription-replication complexes in vivo. J Gen Virol. 1997;78 (Pt 10):2447-51.

875 57. Min JY, Li S, Sen GC, Krug RM. A site on the influenza A virus NS1 protein mediates both
876 inhibition of PKR activation and temporal regulation of viral RNA synthesis. Virology.
877 2007;363(1):236-43.
878 58. Robb NC, Smith M, Vreede FT, Fodor E. NS2/NEP protein regulates transcription and
879 replication of the influenza virus RNA genome. J Gen Virol. 2009;90(Pt 6):1398-407.
880 59. Perez JT, Varble A, Sachidanandam R, Zlatev I, Manoharan M, Garcia-Sastre A, et al.
881 Influenza A virus-generated small RNAs regulate the switch from transcription to replication.
882 Proc Natl Acad Sci U S A. 2010;107(25):11525-30.
883 60. Umbach JL, Yen HL, Poon LL, Cullen BR. Influenza A virus expresses high levels of an
884 unusual class of small viral leader RNAs in infected cells. mBio. 2010;1(4).
885 61. Perez JT, Zlatev I, Aggarwal S, Subramanian S, Sachidanandam R, Kim B, et al. A small-
886 RNA enhancer of viral polymerase activity. J Virol. 2012;86(24):13475-85.
887 62. Olson AC, Rosenblum E, Kuchta RD. Regulation of influenza RNA polymerase activity
888 and the switch between replication and transcription by the concentrations of the vRNA 5'
889 end, the cap source, and the polymerase. Biochemistry. 2010;49(47):10208-15.
890 63. Jorba N, Juarez S, Torreira E, Gastaminza P, Zamarreno N, Albar JP, et al. Analysis of the
891 interaction of influenza virus polymerase complex with human cell factors. Proteomics.
892 2008;8(10):2077-88.
893 64. Mayer D, Molawi K, Martinez-Sobrido L, Ghanem A, Thomas S, Baginsky S, et al.
894 Identification of cellular interaction partners of the influenza virus ribonucleoprotein complex
895 and polymerase complex using proteomic-based approaches. J Proteome Res. 2007;6(2):672-
896 82.
897 65. Watanabe T, Kawakami E, Shoemaker JE, Lopes TJ, Matsuoka Y, Tomita Y, et al.
898 Influenza virus-host interactome screen as a platform for antiviral drug development. Cell Host
899 Microbe. 2014;16(6):795-805.
900 66. Sugiyama K, Kawaguchi A, Okuwaki M, Nagata K. pp32 and APRIL are host cell-derived
901 regulators of influenza virus RNA synthesis from cRNA. Elife. 2015;4.
902 67. Carrique L, Fan H, Walker AP, Keown JR, Sharps J, Staller E, et al. Host ANP32A mediates
903 the assembly of the influenza virus replicase. Nature. 2020;587(7835):638-43.
904 68. Staller E, Sheppard CM, Neasham PJ, Mistry B, Peacock TP, Goldhill DH, et al. ANP32
905 Proteins Are Essential for Influenza Virus Replication in Human Cells. J Virol. 2019;93(17).
906 69. Zhang H, Zhang Z, Wang Y, Wang M, Wang X, Zhang X, et al. Fundamental Contribution
907 and Host Range Determination of ANP32A and ANP32B in Influenza A Virus Polymerase
908 Activity. J Virol. 2019;93(13).
909 70. Jackson DA, Caton AJ, McCready SJ, Cook PR. Influenza virus RNA is synthesized at fixed
910 sites in the nucleus. Nature. 1982;296(5855):366-8.
911 71. Takizawa N, Watanabe K, Nouno K, Kobayashi N, Nagata K. Association of functional
912 influenza viral proteins and RNAs with nuclear chromatin and sub-chromatin structure.
913 Microbes Infect. 2006;8(3):823-33.
914 72. Chase GP, Rameix-Welti MA, Zvirbliene A, Zvirblis G, Gotz V, Wolff T, et al. Influenza
915 virus ribonucleoprotein complexes gain preferential access to cellular export machinery
916 through chromatin targeting. PLoS Pathog. 2011;7(9):e1002187.
917 73. Ver LS, Marcos-Villar L, Landeras-Bueno S, Nieto A, Ortin J. The Cellular Factor
918 NXP2/MORC3 Is a Positive Regulator of Influenza Virus Multiplication. J Virol.
919 2015;89(19):10023-30.
920 74. Alfonso R, Lutz T, Rodriguez A, Chavez JP, Rodriguez P, Gutierrez S, et al. CHD6
921 chromatin remodeler is a negative modulator of influenza virus replication that relocates to
922 inactive chromatin upon infection. Cell Microbiol. 2011;13(12):1894-906.

923 75. Marcos-Villar L, Pazo A, Nieto A. Influenza Virus and Chromatin: Role of the CHD1
924 Chromatin Remodeler in the Virus Life Cycle. J Virol. 2016;90(7):3694-707.
925 76. Rodriguez A, Perez-Gonzalez A, Nieto A. Cellular human CLE/C14orf166 protein
926 interacts with influenza virus polymerase and is required for viral replication. J Virol.
927 2011;85(22):12062-6.
928 77. Mahmoudabadi G, Milo R, Phillips R. Energetic cost of building a virus. Proc Natl Acad
929 Sci U S A. 2017;114(22):E4324-E33.
930 78. Laussel C, Leon S. Cellular toxicity of the metabolic inhibitor 2-deoxyglucose and
931 associated resistance mechanisms. Biochem Pharmacol. 2020;182:114213.
932 79. Gualdoni GA, Mayer KA, Kapsch AM, Kreuzberg K, Puck A, Kienzl P, et al. Rhinovirus
933 induces an anabolic reprogramming in host cell metabolism essential for viral replication. Proc
934 Natl Acad Sci U S A. 2018;115(30):E7158-E65.
935 80. Vijayaraghavan R, Kumar D, Dube SN, Singh R, Pandey KS, Bag BC, et al. Acute toxicity
936 and cardio-respiratory effects of 2-deoxy-D-glucose: a promising radio sensitiser. Biomed
937 Environ Sci. 2006;19(2):96-103.
938 81. Chiaravalli M, Rowe I, Mannella V, Quilici G, Canu T, Bianchi V, et al. 2-Deoxy-d-Glucose
939 Ameliorates PKD Progression. J Am Soc Nephrol. 2016;27(7):1958-69.
940 82. Kovarik JJ, Kernbauer E, Holzl MA, Hofer J, Gualdoni GA, Schmetterer KG, et al. Fasting
941 metabolism modulates the interleukin-12/interleukin-10 cytokine axis. PLoS One.
942 2017;12(7):e0180900.
943 83. Stein M, Lin H, Jeyamohan C, Dvorzhinski D, Gounder M, Bray K, et al. Targeting tumor
944 metabolism with 2-deoxyglucose in patients with castrate-resistant prostate cancer and
945 advanced malignancies. Prostate. 2010;70(13):1388-94.
946 84. Raez LE, Papadopoulos K, Ricart AD, Chiorean EG, Dipaola RS, Stein MN, et al. A phase
947 I dose-escalation trial of 2-deoxy-D-glucose alone or combined with docetaxel in patients with
948 advanced solid tumors. Cancer Chemother Pharmacol. 2013;71(2):523-30.
949 85. Sahu KK, Kumar R. Role of 2-Deoxy-D-Glucose (2-DG) in COVID-19 disease: A potential
950 game-changer. J Family Med Prim Care. 2021;10(10):3548-52.
951 86. Bhatt AN, Shenoy S, Munjal S, Chinnadurai V, Agarwal A, Vinoth Kumar A, et al. 2-
952 deoxy-D-glucose as an adjunct to standard of care in the medical management of COVID-19:
953 a proof-of-concept and dose-ranging randomised phase II clinical trial. BMC Infect Dis.
954 2022;22(1):669.
955 87. Wang A, Huen SC, Luan HH, Yu S, Zhang C, Gallezot JD, et al. Opposing Effects of Fasting
956 Metabolism on Tissue Tolerance in Bacterial and Viral Inflammation. Cell. 2016;166(6):1512-
957 25 e12.
958 88. Chou SH, Kojic LD, Messingham KN, Cunnic JE. Characterization of the effect of 2-
959 deoxy-D-glucose(2-DG) on the immune system. Brain Behav Immun. 1996;10(4):399-416.
960 89. Hansen IL, Levy MM, Kerr DS. The 2-deoxyglucose test as a supplement to fasting for
961 detection of childhood hypoglycemia. Pediatr Res. 1984;18(4):359-64.
962 90. Pajak B, Zielinski R, Manning JT, Matejin S, Paessler S, Fokt I, et al. The Antiviral Effects
963 of 2-Deoxy-D-glucose (2-DG), a Dual D-Glucose and D-Mannose Mimetic, against SARS-CoV-2
964 and Other Highly Pathogenic Viruses. Molecules. 2022;27(18).
965 91. Matos ADR, Wunderlich K, Schloer S, Schughart K, Geffers R, Seders M, et al. Antiviral
966 potential of human IFN-alpha subtypes against influenza A H3N2 infection in human lung
967 explants reveals subtype-specific activities. Emerg Microbes Infect. 2019;8(1):1763-76.
968 92. Hoffmann E, Stech J, Guan Y, Webster RG, Perez DR. Universal primer set for the full-
969 length amplification of all influenza A viruses. Arch Virol. 2001;146(12):2275-89.

970 93. Livak KJ, Schmittgen TD. Analysis of relative gene expression data using real-time
971 quantitative PCR and the 2(-Delta Delta C(T)) Method. Methods. 2001;25(4):402-8.
972

973

Fig 1: 2-DG impairs IAV propagation and is well tolerated by A549 cells. (A+B) 24 h after seeding, A549 cells were infected with SC35M at an MOI of 0.001 for 30 min and incubated in the presence of 25 mM glucose and the indicated concentrations of 2-DG or its solvent water for **(A)** 24 h or **(B)** 24 and 48 h. Subsequently, supernatants were collected to determine viral titers via plaque assay. **(C)** Uninfected cells were treated with the indicated inhibitor concentrations for 24 h and were then subjected to LDH assay for assessment of the relative cytotoxicity of the treatment. **(D-F)** The glycolytic proton efflux rate (glycoPER), extracellular acidification rate (ECAR) and oxygen consumption rate (OCR) were measured in real-time via glycolytic rate assay and a Seahorse XFe96 Analyzer. The kinetics show the influence of different concentrations of 2-DG on the three measured parameters. Depicted are the means ± SD of **(A-C)** three or **(D-F)** five independent experiments with **(A-C)** three or **(D-F)** four biological replicates per condition and experiment. Statistical significances were determined via **(A)** unpaired one-way ANOVA and Dunnett's correction, comparing all treated samples to the water control and **(B-F)** ordinary two-way ANOVA with **(B)** Tukey's, **(C)** Sidak's and **(D-F)** Dunnett's correction for multiple comparison, comparing **(B)** all samples with one another, **(C)** all treated samples of one group to the respective water control or **(D-F)** the time points of differentially treated cells with their respective start value. p-values are indicated as follows: < 0.05 = *, < 0.01 = **, < 0.001 = ***, < 0.0001 = ****.

Fig 2: 2-DG mildly reduces the expression of viral proteins. (A+B) 24 h after seeding, A549 cells were infected with SC35M at the depicted MOIs for 30 min and were incubated with 25 mM glucose and the indicated concentrations of 2-DG for a total of **(A)** 24 h or **(B)** 8 h. Lysates of triplicates were unified to yield sufficient protein amounts. Proteins were separated via SDS-PAGE. Visualization was done using primary antibodies against PA (rabbit), M1 (mouse), NP (rabbit), NS1 (rabbit) and ERK2 (rabbit) and fluorescence-labelled anti-mouse (donkey) and anti-rabbit (donkey) secondary antibodies. Depicted are representative protein bands from three independent experiments. **(C)** HEK293T cells were, 24 h after seeding, transfected with an empty vector or a plasmid containing the *Renilla* luciferase gene which is under the control of a constitutive herpes simplex virus thymidine kinase promoter. Subsequently, the cells were incubated with the shown 2-DG concentrations. After 24 h, cells were lysed and the n-fold of relative light units (RLU) in comparison to the water control was measured via luciferase assay. Depicted are the means ± SD of three independent experiments with three biological replicates per condition and experiment. Statistical significances were determined via unpaired one-way ANOVA and Dunnett's correction, comparing all treated samples to the water control. p-values are indicated as follows: < 0.05 = *, < 0.01 = **, < 0.001 = ***, < 0.0001 = ****.

Fig 3: 2-DG conversely affects IAV mRNA and vRNA accumulation. 24 h after seeding, A549 cells were infected with SC35M at the depicted MOIs for 30 min and were incubated with 25 mM glucose and the indicated concentrations of 2-DG for a total of **(A+B)** 24 h or **(C+D)** 8 h. Subsequently, cells were lysed, their RNA isolated and cDNA synthesized using either **(A+C)** oligo(dT) primers to transcribe mRNA or **(B+D)** fluA uni12 primers to transcribe vRNA. Real-time qPCR was performed with two technical replicates per sample and values of treated samples were normalized to the water control. In case of mRNA detection, all results were additionally normalized to a GAPDH control. Depicted are the means ± SD of three independent experiments with three biological replicates per condition and experiment. Statistical significances were determined via unpaired one-way ANOVA and Dunnett's correction, comparing all treated samples to the water control. p-values are indicated as follows: < 0.05 = *, < 0.01 = **, < 0.001 = ***, < 0.0001 = ****.

Fig 4: Prolongation of IAV transcription and reduction of replication by 2-DG. 24 h after seeding, A549 cells were infected with SC35M at an MOI of 5 for 30 min and were incubated without or with 10 mM 2-DG in the presence of 25 mM glucose for a total of 8 h. **(A+B)** Each hour or **(C-H)** 8 hpi cells were lysed, their RNA isolated and cDNA synthesized using **(A)** oligo(dT) primers, **(B)** fluA uni12 primers or **(C-H)** specific primers to transcribe mRNA and vRNA of the SC35M gene segments 1 (PB2), 5 (NP) and 6 (NA). Real-time qPCR was performed with two technical replicates per sample. **(A+B)** All values were normalized to the water control 1 hpi or **(C-H)** values of treated samples were normalized to the water control. Depicted are the means ± SD of three independent experiments with three biological replicates per condition and experiment. Statistical significances were determined **(A+B)** via ordinary two-way ANOVA and Sidak's correction, comparing the treated sample of each time point to its respective water control or **(C-H)** via unpaired t-test. p-values are indicated as follows: < 0.05 = *, < 0.01 = **, < 0.001 = ***, < 0.0001 = ****.

Fig 5: 2-DG shows no effect on the replicative capacity of the IAV polymerase. 24 h after seeding, HEK293T cells were transfected with plasmids encoding PA, PB1, PB2 and NP of SC35M, the transfection control *Renilla* luciferase and either a **(A)** vRNA-like or **(B)** cRNA-like template of the *Firefly* luciferase. The negative control was transfected with an empty vector instead of PB2. 4 h later the transfection solution was replaced with medium containing 25 mM glucose and the indicated concentrations of 2-DG for another 20 h. Subsequently, cells were lysed and the n-fold of relative light units (RLU) was measured via luciferase assay and normalized to the water control. Additionally, all values were normalized to their respective transfection control. Statistical significances were determined via unpaired one-way ANOVA and Dunnett's correction, comparing all other samples to the water control. p-values are indicated as follows: < 0.05 = *, < 0.01 = **, < 0.001 = ***, < 0.0001 = ****.

Fig 6: Metabolic alterations induced by IAV infection and glycolytic treatment. A549 cells were mock-infected or infected with SC35M at an MOI of 0.001 and were subsequently incubated in DMEM (containing 25 mM glucose) with or without 10 mM 2-DG and 1 mM mannose as indicated. 24 hpi metabolic activity was quenched and intracellular metabolites were relatively quantified via HILIC-MS/MS. All values have been normalized to the uninfected and untreated control (left column). Darker shades of blue indicate a higher and darker shades of red indicate a lower n-fold of the respective metabolite compared to the control. Black indicates increases higher than 5-fold compared to the control. Depicted are the means of three independent experiments with three biological replicates per condition and experiment. Statistical significances were determined via ordinary two-way ANOVA and Dunnett's correction, comparing all samples to their respective uninfected and untreated control. The n-folds and p-values are presented in **Table S1**.

Fig 7: Mannose counteracts 2-DG by refueling glycolysis. (A) The metabolic pathways of glycolysis and *N*-linked glycosylation are closely connected via mannose-6-phosphate isomerase (MPI). Other enzymes depicted here are hexokinase (HK), glucose-6-phosphate isomerase (GPI), and phosphomannomutase 2 (PMM2). **(B-D)** 24 h after seeding, A549 cells were infected with SC35M at an MOI of **(B)** 0.001 or **(C+D)** 5 for 30 min and were incubated with 25 mM glucose and the indicated concentrations of 2-DG, mannose, and the mannose-6 phosphate isomerase inhibitor MLS0315771 (MLS) for a total of **(B)** 24 h or **(C+D)** 8 h. Subsequently, **(B)** supernatants were collected to determine viral titers via plaque assay or **(C+D)** cells were lysed, their RNA isolated and cDNA synthesized using either **(C)** fluA uni12 primers to transcribe vRNA or **(D)** oligo(dT) primers to transcribe mRNA. Real-time qPCR was performed with two technical replicates per sample and values of treated samples were normalized to the untreated control. In case of mRNA detection all results were additionally normalized to a GAPDH control. Depicted are the means ± SD of three independent experiments with three biological replicates per condition and experiment. Statistical

significances were determined via unpaired one-way ANOVA and Dunnett's correction, comparing all treated samples to the untreated control. p-values are indicated as follows: < 0.05 = *, < 0.01 = **, < 0.001 = ***, < 0.0001 = ****.

Fig S1: Effects of 2-DG on IAV propagation, cell growth and immune induction. 24 h after seeding, A549 cells were infected with SC35M at an MOI of **(A+B)** 0.01 or **(C+D)** 0.001 for 30 min and incubated in the presence of the indicated concentrations of 2-DG or its solvent water for 24 h. Subsequently, cells were **(A+B)** stained with an NP antibody and a live/dead marker and analyzed via flow cytometry or **(C+D)** detached to assess the number of living cells as well as the viability via trypan blue exclusion in an automated cell counter. **(E-H)** Uninfected cells were transfected with cellular or viral RNA and treated with the indicated 2-DG concentrations for 6 h. Subsequently, cells were lysed, their RNA isolated and cDNA synthesized using oligo(dT) primers to transcribe mRNA. Real-time qPCR was performed with two technical replicates per sample and values of all other samples were normalized to the unstimulated water control. Additionally, all results were normalized to a GAPDH control. **(A-H)** Depicted are the means ± SD of three independent experiments with three biological replicates per condition and experiment. Statistical significances were determined via **(A, C, D)** unpaired one-way ANOVA and Dunnett's correction, comparing all treated samples to the water control or **(B, E-H)** ordinary two-way ANOVA with Dunnett's correction, comparing all treated samples of both groups to their respective water control. p-values are indicated as follows: < 0.05 = *, < 0.01 = **, < 0.001 = ***, < 0.0001 = ****.

Fig S2: Effects of 2-DG on human primary cells and IAV propagation. (A) Human lung explants were infected with 2 x 10^5 SC35M particles for 30 min. Afterwards they were incubated with 11.1 mM glucose and the indicated concentrations of 2-DG and supernatants were collected 1, 24 and 48 hpi to determine viral titers via plaque assay. **(B-I)** After reaching ≈ 90 % confluency **(B)** uninfected HBEpCs were treated with the indicated concentrations of 2-DG or its solvent water for 24 h. Afterwards the supernatants were used to perform LDH assays to determine the relative cytotoxicity of the treatment. **(C-I)** HBEpCs were infected with SC35M at an MOI of **(C)** 1, **(D, F, H)** 0.01 or **(E, G, I)** 5 for 30 min and were incubated with 6 mM glucose and the indicated concentrations of 2-DG for a total of **(D, F, H)** 24 h or **(E, G, I)** 8 h. Subsequently, **(C-E)** supernatants were used to **(C)** perform lactate assays in order to indirectly assess the glycolytic activity and **(D+E)** determine viral titers via plaque assay. **(F-I)** Additionally, cells were lysed, their RNA isolated and cDNA synthesized using either **(F+H)** oligo(dT) primers to transcribe mRNA or **(H+I)** fluA uni12 primers to transcribe vRNA. Real-time qPCR was performed with two technical replicates per sample and values of treated samples were normalized to the water control. In case of mRNA detection, all results were additionally normalized to a GAPDH control. Depicted are the means ± SD of three independent experiments with three biological replicates per condition and experiment. Statistical significances were determined via **(A-C)** ordinary two-way ANOVA and Dunnett's correction, comparing each treated sample to its respective water control. **(D-I)** Other significances were determined via unpaired one-way ANOVA and Dunnett's correction, comparing all treated samples to the water control. p-values are indicated as follows: < 0.05 = *, < 0.01 = **, < 0.001 = ***, < 0.0001 = ****.

Fig S3: Impairment of IAV replication by 2-DG is not strain-specific. 24 h after seeding, A549 cells were infected with Pan/99 at the depicted MOIs for 30 min and were incubated with the indicated concentrations of 2-DG or its solvent water for a total of **(A-C)** 24 h or **(D+E)** 8 h. Subsequently, **(A)** supernatants were collected to determine viral titers via plaque assay or **(B-E)** cells were lysed, their RNA isolated and cDNA synthesized using either **(B+D)** oligo(dT) primers to transcribe mRNA or **(C+E)** fluA uni12 primers to transcribe vRNA. Real-time qPCR was performed with two technical replicates per sample and values of treated samples were normalized to the water control. In case of mRNA detection, all results were additionally normalized to a GAPDH control. Depicted are the means ± SD of three independent experiments with three biological replicates per condition and experiment. Statistical significances were determined via unpaired one-way ANOVA and Dunnett's correction, comparing all treated samples to the water control. p-values are indicated as follows: < 0.05 = *, < 0.01 = **, < 0.001 = ***, < 0.0001 = ****.

Fig S4: 2-DG does not impair IAV vRNA durability. 24 h after seeding, HEK293T cells were transfected with plasmids containing the SC35M sequences of PA, PB1, PB2 and NP. 4 h later the transfection solution was replaced with fresh medium for another 20 h. Subsequently, cells were infected with SC35M at an MOI of 5 for 30 min and were incubated with the indicated concentrations of 2-DG and 100 µg/mL cycloheximide. A negative control was previously transfected with an empty vector instead of PA while a positive control was not treated with cycloheximide. 6 hpi, cells were lysed, their RNA isolated and cDNA synthesized using specific primers to transcribe vRNA of the SC35M gene segment 6 (NA). Real-time qPCR was performed with two technical replicates per sample. Statistical significances were determined via unpaired one-way ANOVA and Dunnett's correction, comparing all other samples to the water control. p-values are indicated as follows: < 0.05 = *, < 0.01 = **, < 0.001 = ***, < 0.0001 = ****.

Fig S5: Effects of mannose, MLS0315771, and pyruvate on IAV propagation and A549 cells. 24 h after seeding, A549 cells were infected with SC35M at an MOI of 0.001 or for 30 min and incubated in the presence of the indicated concentrations of metabolites and inhibitors or their solvents for a total of 24 h. Subsequently, **(A, D-F)** supernatants were collected to determine **(A, E, F)** viral titers via plaque assay and **(D)** extracellular lactate concentrations via lactate assay or **(B+C)** cells were detached to assess the number of living cells and the viability via trypan blue exclusion and an automated cell counter. Depicted are the means ± SD of three independent experiments with three biological replicates per condition and experiment. Statistical significances were determined via unpaired one-way ANOVA and Dunnett's correction, comparing **(B-E)** all treated samples to the DMSO control or **(A+F)** all other samples to the 2-DG-treated sample (white bar). p-values are indicated as follows: < 0.05 = *, < 0.01 = **, < 0.001 = ***, < 0.0001 = ****.

Fig S6: Gating strategy for the quantification of uninfected versus infected and living versus dead cells. A549 cells were infected with SC35M at an MOI of 0.01. Directly after the infection, cells were mock-treated or treated with 2-DG. 24 hpi cells were stained with a viability dye and an NP antibody and were quantified via flow cytometry. At first cells were pre-gated according to their FSC/SSC appearance. Then these cells were sub-classified to discriminate between uninfected and infected cells as well as living and dead cells. Representative dot plots are depicted to exemplify the gating strategy used for data analysis in Fig S1A+B.

Table S1: n-fold changes over control and statistical significances of Fig 6.

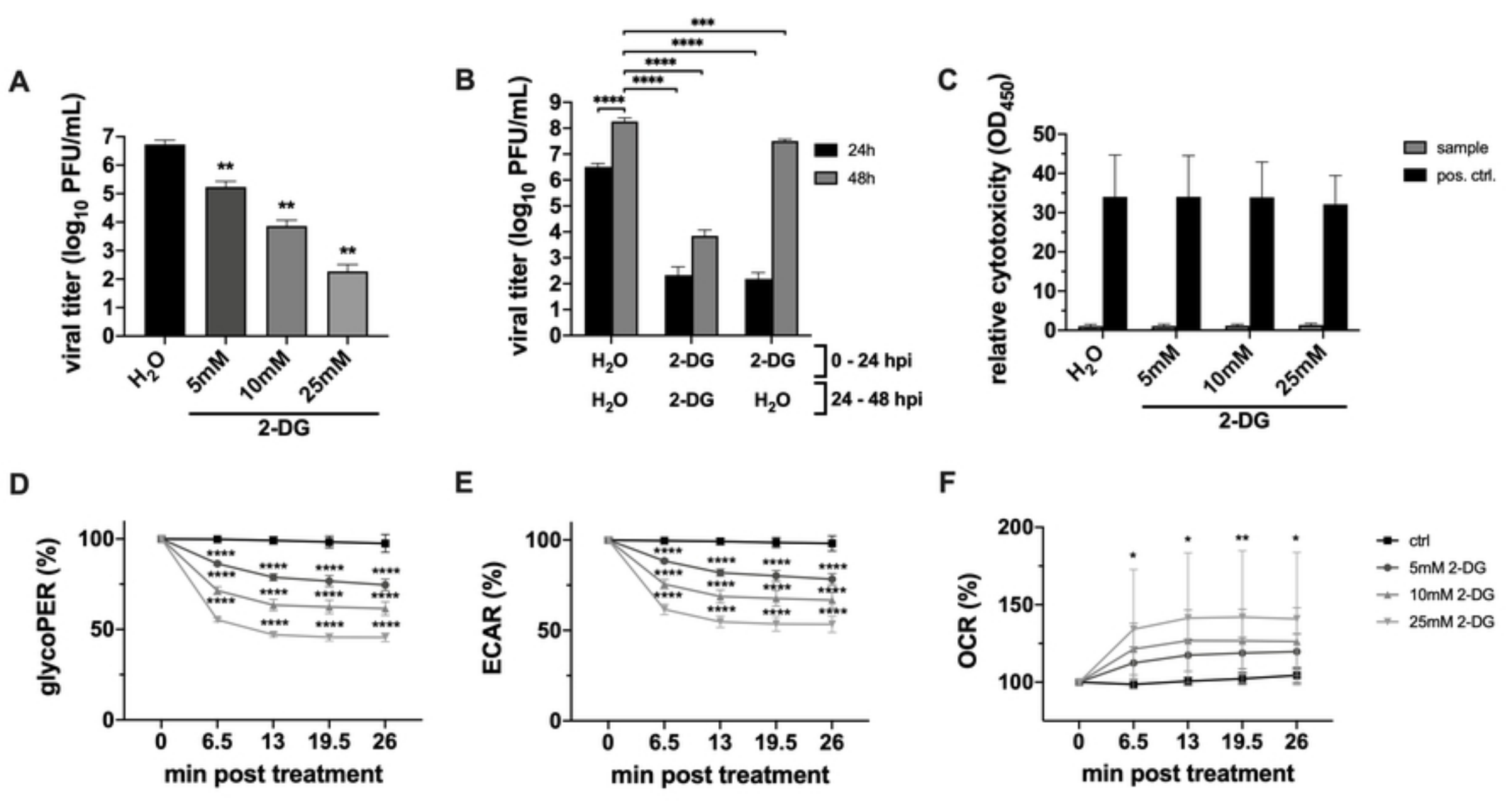
A
viral titer (log10 PFU/mL)
H2O
5mM
10mM
25mM
2-DG
B
viral titer (log10 PFU/mL)
24h
48h
H2O
2-DG
2-DG
0 - 24 hpi
H2O
2-DG
H2O
24 - 48 hpi
C
relative cytotoxicity (OD450)
sample
pos. ctrl.
H2O
5mM
10mM
25mM
2-DG
D
glycoPER (%)
min post treatment
E
ECAR (%)
min post treatment
F
OCR (%)
min post treatment
ctrl
5mM 2-DG
10mM 2-DG
25mM 2-DG

Fig 1

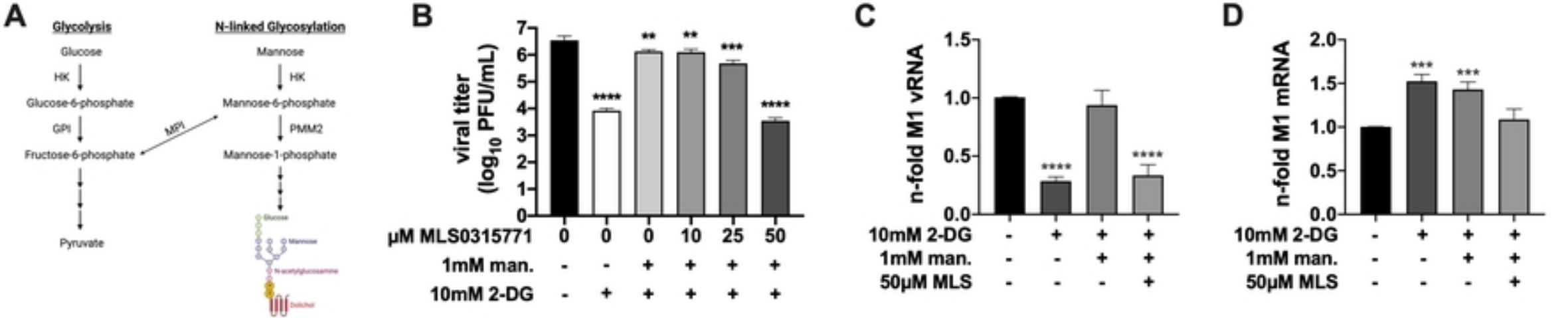
A
Glycolysis
Glucose
HK
Glucose-6-phosphate
GPI
Fructose-6-phosphate
Pyruvate
MPI
N-linked Glycosylation
Mannose
HK
Mannose-6-phosphate
PMM2
Mannose-1-phosphate
Glucose
Mannose
N-acetylglucosamine
Dolichol
B
viral titer (log10 PFU/mL)
μM MLS0315771 0 0 0 10 25 50
1mM man. - - + + + +
10mM 2-DG - + + + + +
C
n-fold M1 vRNA
10mM 2-DG - + + +
1mM man. - - + +
50μM MLS - - - +
D
n-fold M1 mRNA
10mM 2-DG - + + +
1mM man. - - + +
50μM MLS - - - +

Fig 7

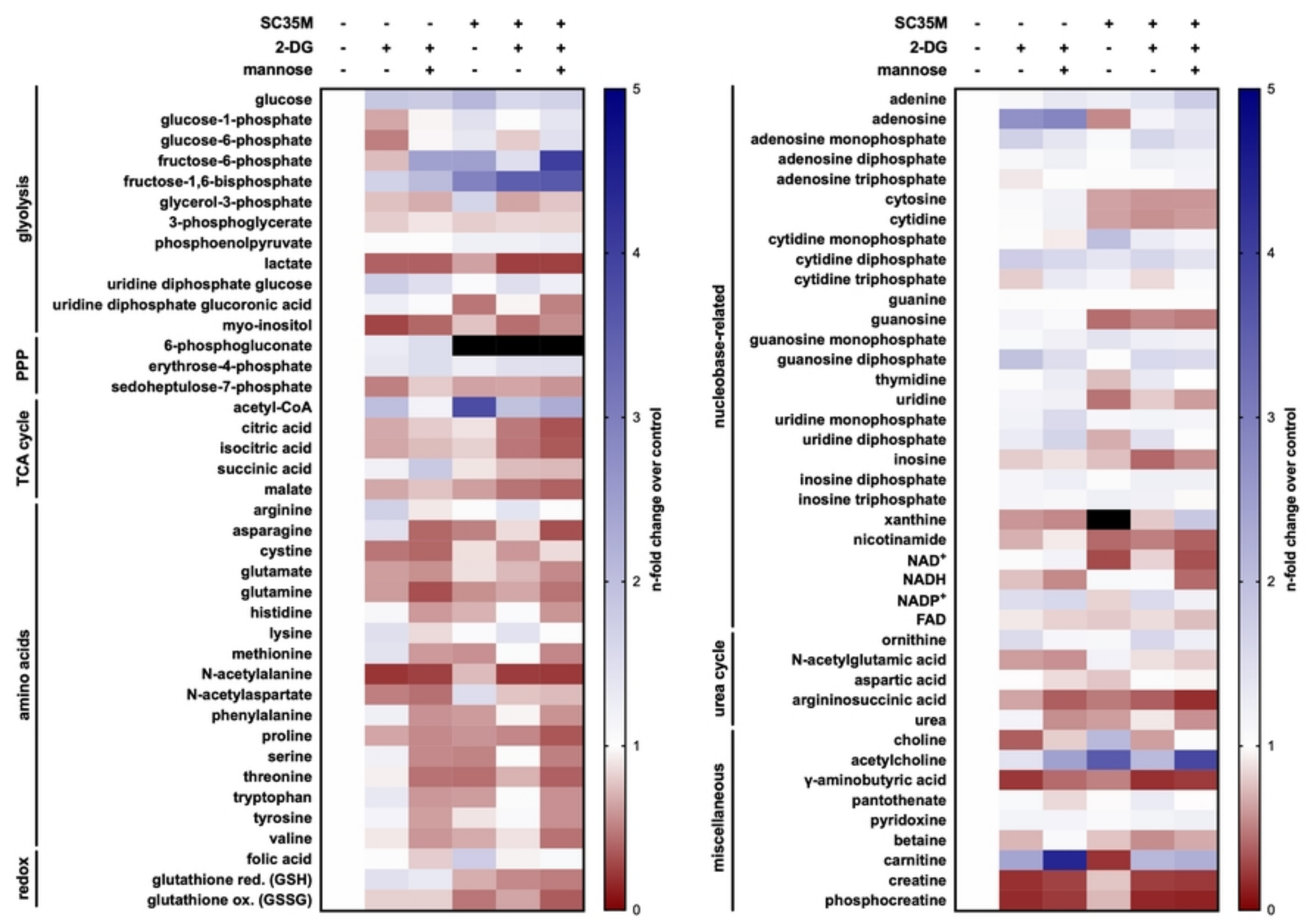
SC35M - - - + + +
2-DG - + + - + +
mannose - - + - - +
glycolysis
glucose
glucose-1-phosphate
glucose-6-phosphate
fructose-6-phosphate
fructose-1,6-bisphosphate
glycerol-3-phosphate
3-phosphoglycerate
phosphoenolpyruvate
lactate
uridine diphosphate glucose
uridine diphosphate glucoronic acid
myo-inositol
PPP
6-phosphogluconate
erythrose-4-phosphate
sedoheptulose-7-phosphate
TCA cycle
acetyl-CoA
citric acid
isocitric acid
succinic acid
malate
amino acids
arginine
asparagine
cystine
glutamate
glutamine
histidine
lysine
methionine
N-acetylalanine
N-acetylaspartate
phenylalanine
proline
serine
threonine
tryptophan
tyrosine
valine
redox
folic acid
glutathione red. (GSH)
glutathione ox. (GSSG)
n-fold change over control
0
1
2
3
4
5
SC35M - - - + + +
2-DG - + + - + +
mannose - - + - - +
nucleobase-related
adenine
adenosine
adenosine monophosphate
adenosine diphosphate
adenosine triphosphate
cytosine
cytidine
cytidine monophosphate
cytidine diphosphate
cytidine triphosphate
guanine
guanosine
guanosine monophosphate
guanosine diphosphate
thymidine
uridine
uridine monophosphate
uridine diphosphate
inosine
inosine diphosphate
inosine triphosphate
xanthine
nicotinamide
NAD+
NADH
NADP+
FAD
urea cycle
ornithine
N-acetylglutamic acid
aspartic acid
argininosuccinic acid
urea
miscellaneous
choline
acetylcholine
γ-aminobutyric acid
pantothenate
pyridoxine
betaine
carnitine
creatine
phosphocreatine
n-fold change over control
0
1
2
3
4
5

Fig 6

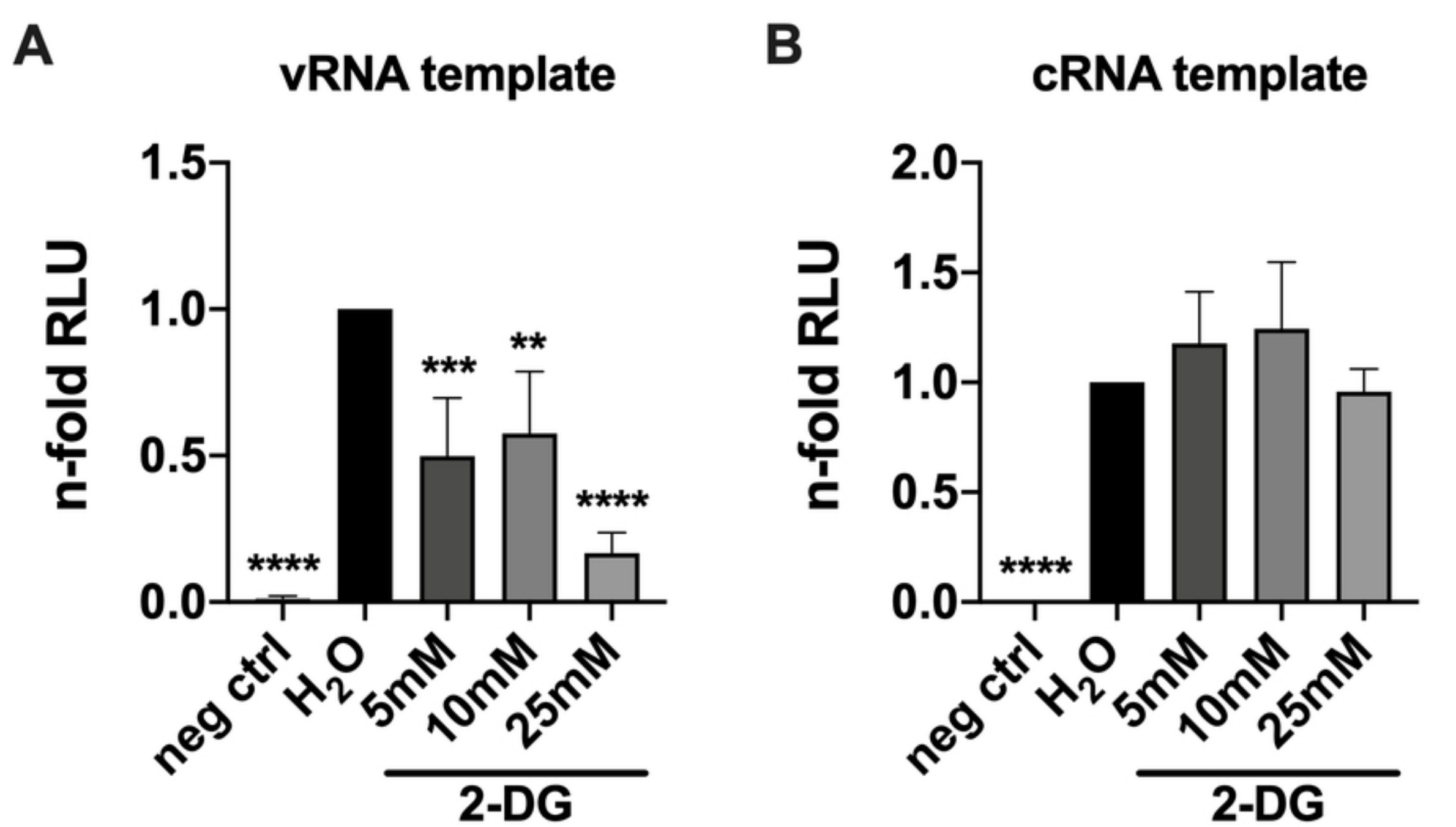
A
vRNA template
n-fold RLU
1.5
1.0
0.5
0.0
****
***
**
****
neg ctrl
H2O
5mM
10mM
25mM
2-DG
B
cRNA template
n-fold RLU
2.0
1.5
1.0
0.5
0.0
****
neg ctrl
H2O
5mM
10mM
25mM
2-DG

Fig 5

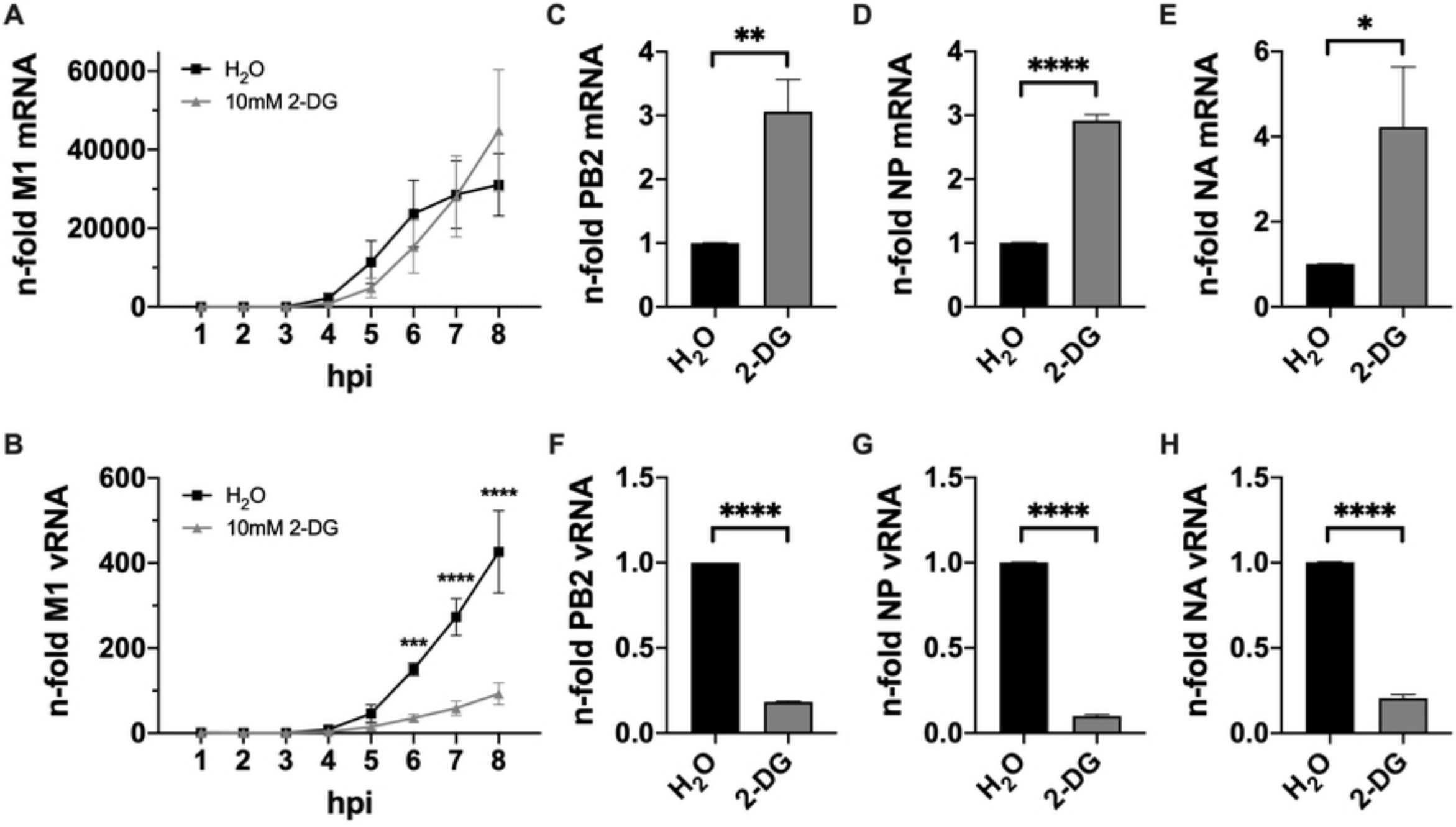
A
n-fold M1 mRNA
60000
40000
20000
0
H2O
10mM 2-DG
1 2 3 4 5 6 7 8
hpi
C
n-fold PB2 mRNA
**
4
3
2
1
0
H2O
2-DG
D
n-fold NP mRNA
****
4
3
2
1
0
H2O
2-DG
E
n-fold NA mRNA
*
6
4
2
0
H2O
2-DG
B
n-fold M1 vRNA
600
400
200
0
H2O
10mM 2-DG
***
****
****
1 2 3 4 5 6 7 8
hpi
F
n-fold PB2 vRNA
****
1.5
1.0
0.5
0.0
H2O
2-DG
G
n-fold NP vRNA
****
1.5
1.0
0.5
0.0
H2O
2-DG
H
n-fold NA vRNA
****
1.5
1.0
0.5
0.0
H2O
2-DG

Fig 4

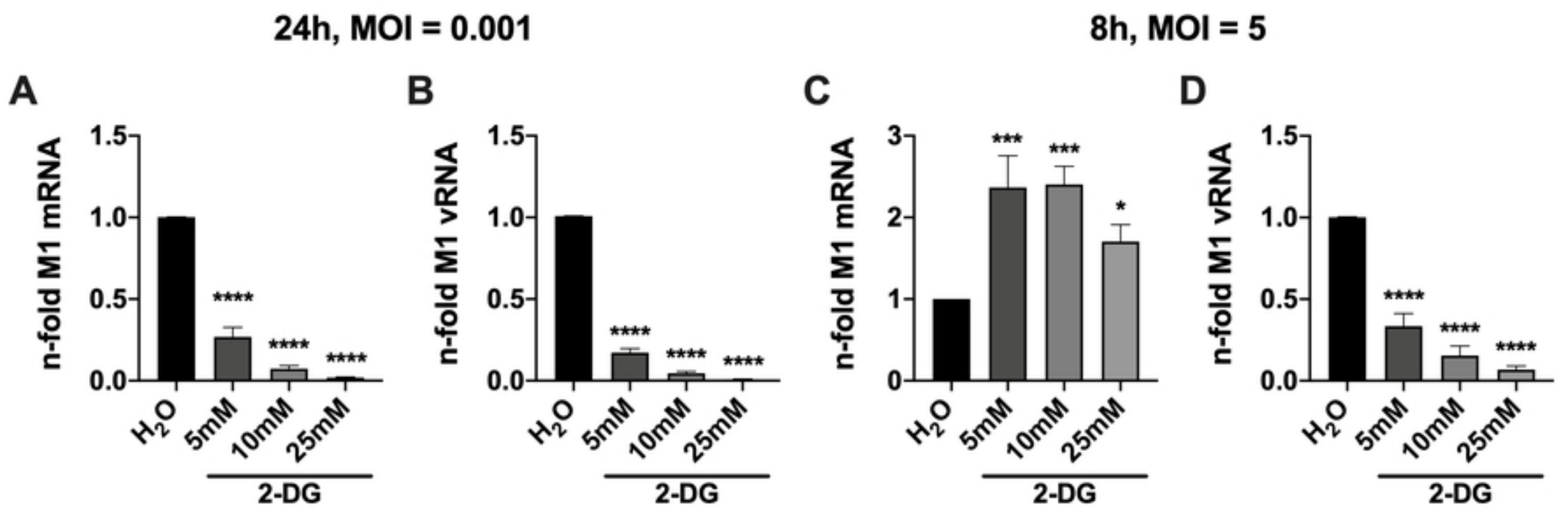
24h, MOI = 0.001
8h, MOI = 5
A
B
C
D
n-fold M1 mRNA
n-fold M1 vRNA
n-fold M1 mRNA
n-fold M1 vRNA
1.5
1.0
0.5
0.0
3
2
1
0
****
***
*
H2O
5mM
10mM
25mM
2-DG

Fig 3

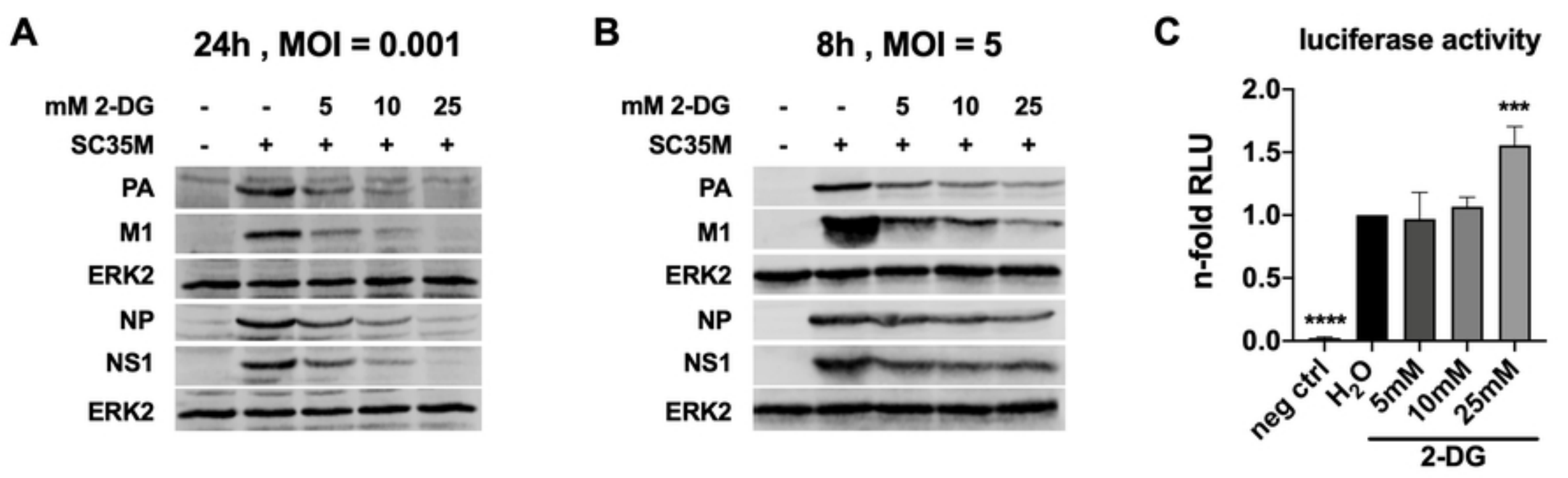
A
24h , MOI = 0.001
mM 2-DG - - 5 10 25
SC35M - + + + +
PA
M1
ERK2
NP
NS1
ERK2
B
8h , MOI = 5
mM 2-DG - - 5 10 25
SC35M - + + + +
PA
M1
ERK2
NP
NS1
ERK2
C
luciferase activity
n-fold RLU
2.0
1.5
1.0
0.5
0.0
****
***
neg ctrl
H2O
5mM
10mM
25mM
2-DG

Fig 2